




## RESEARCH ARTICLE

# Beyond “greening” and “browning”: Trends in grassland ground cover fractions across Eurasia that account for spatial and temporal autocorrelation

Katarzyna Ewa Lewińska<sup>1</sup>  | Anthony R. Ives<sup>2</sup>  | Clay J. Morrow<sup>2,3</sup>  |  
 Natalia Rogova<sup>1</sup>  | He Yin<sup>4</sup>  | Paul R. Elsen<sup>5</sup>  | Kirsten de Beurs<sup>6</sup>  |  
 Patrick Hostert<sup>7,8</sup>  | Volker C. Radeloff<sup>1</sup> 

<sup>1</sup>SILVIS Lab, Department of Forest and Wildlife Ecology, University of Wisconsin-Madison, Madison, Wisconsin, USA

<sup>2</sup>Department of Integrative Biology, University of Wisconsin-Madison, Madison, Wisconsin, USA

<sup>3</sup>Department of Forest and Wildlife Ecology, University of Wisconsin-Madison, Madison, Wisconsin, USA

<sup>4</sup>Department of Geography, Kent State University, Kent, Ohio, USA

<sup>5</sup>Global Conservation Program, Wildlife Conservation Society, Bronx, New York, USA

<sup>6</sup>Laboratory of Geo-Information Science and Remote Sensing, Wageningen University & Research, Wageningen, the Netherlands

<sup>7</sup>Geography Department, Humboldt-Universität zu Berlin, Berlin, Germany

<sup>8</sup>Integrative Research Institute on Transformations of Human-Environment Systems (IRI THESys), Humboldt-Universität zu Berlin, Berlin, Germany

## Correspondence

Katarzyna Ewa Lewińska, SILVIS Lab, Department of Forest and Wildlife Ecology, University of Wisconsin-Madison, 1630 Linden Drive, Madison, WI 53706, USA.  
 Email: [lewinska@wisc.edu](mailto:lewinska@wisc.edu)

## Present address

Katarzyna Ewa Lewińska, Geography Department, Humboldt-Universität zu Berlin, Berlin, Germany

## Abstract

Grassland ecosystems cover up to 40% of the global land area and provide many ecosystem services directly supporting the livelihoods of over 1 billion people. Monitoring long-term changes in grasslands is crucial for food security, biodiversity conservation, achieving Land Degradation Neutrality goals, and modeling the global carbon budget. Although long-term grassland monitoring using remote sensing is extensive, it is typically based on a single vegetation index and does not account for temporal and spatial autocorrelation, which means that some trends are falsely identified while others are missed. Our goal was to analyze trends in grasslands in Eurasia, the largest continuous grassland ecosystems on Earth. To do so, we calculated Cumulative Endmember Fractions (annual sums of monthly ground cover fractions) derived from MODIS 2002–2020 time series, and applied a new statistical approach PARTS that explicitly accounts for temporal and spatial autocorrelation in trends. We examined trends in green vegetation, non-photosynthetic vegetation, and soil ground cover fractions considering their independent change trajectories and relations among fractions over time. We derived temporally uncorrelated pixel-based trend maps and statistically tested whether observed trends could be explained by elevation, land cover, SPEI3, climate, country, and their combinations, all while accounting for spatial autocorrelation. We found no statistical evidence for a decrease in vegetation cover in grasslands in Eurasia. Instead, there was a significant map-level increase in non-photosynthetic vegetation across the region and local increases in green vegetation with a concomitant decrease in soil fraction. Independent environmental variables affected trends significantly, but effects varied by region. Overall, our analyses show in a statistically robust manner that Eurasian grasslands have changed considerably over the past two decades. Our approach enhances remote sensing-based monitoring of trends in grasslands so that underlying processes can be discerned.

This is an open access article under the terms of the [Creative Commons Attribution](https://creativecommons.org/licenses/by/4.0/) License, which permits use, distribution and reproduction in any medium, provided the original work is properly cited.

© 2023 The Authors. *Global Change Biology* published by John Wiley & Sons Ltd.

**Funding information**

Aeronautics Research Mission  
Directorate, Grant/Award Number:  
80NSSC18K0316, 80NSSC18K0343 and  
NASAIAI- 80NSSC20K0282

**KEYWORDS**

arid environments, autoregressive, Cumulative Endmember Fractions, MODIS, PARTS, remotePARTS, spectral mixture analysis, spectral unmixing, steppe, time series

## 1 | INTRODUCTION

Grassland ecosystems cover up to 40% of the global land area and harbor over 30% of the global carbon stored in soils (Bardgett et al., 2021; FAO, 2005; Lorenz & Lal, 2018; Panunzi, 2008). Grasslands also provide many ecosystem services (Bengtsson et al., 2019), support wellbeing of more than 1 billion people, and regulate climate through carbon sequestration and albedo-driven air circulation (Bengtsson et al., 2019; Lioubimtseva & Henebry, 2009; O'Mara, 2012). Anthropogenic and environmental factors influence grasslands at different spatial and temporal scales and may lead to degradation and vegetation recovery (Bardgett et al., 2021; Cherlet et al., 2018; FAO, 2005). While identification of abrupt changes with moderate to high magnitudes and their causes is typically straightforward, detection of subtle changes taking place over longer time periods is more challenging, as is identification of significant drivers causing these trends. Appropriate and statistically valid assessment of changes in grasslands and identification of their drivers is pivotal to support biodiversity, food security, and climate change modeling and mitigation efforts (IPBES, 2018; IPCC, 2019; O'Mara, 2012), including meeting global environmental and development goals (Cowie et al., 2018), and UN ecosystem restoration efforts (UN General Assembly, 2021).

The grasslands of Eurasia are the largest continuous grassland ecosystem on Earth and are instrumental to economy, food security (O'Mara, 2012), global ecology (Baumann et al., 2020; Smelansky & Tishkov, 2012), air circulation (Lioubimtseva & Henebry, 2009), and the carbon cycle (Ni, 2002; Rolinski et al., 2021). However, grassland ecosystems in Eurasia vary considerably (De Keersmaecker et al., 2015; Smelansky & Tishkov, 2012), experience diverse climate change impacts (IPCC, 2019; Lioubimtseva & Henebry, 2009), and have different land use histories (Freitag et al., 2021; Kerven et al., 2021). Since the beginning of the 20th century, grassland ecosystems in Eurasia have sustained several extensive and intensive changes in land cover (Winkler et al., 2021) and land use intensity that have triggered long-term changes, often accelerated by climate change (Jiang et al., 2017). For example, many grasslands in Central Asia were ploughed during the Virgin Lands Campaign in the 1950s and 1960s (Karch et al., 1964; Prishchepov et al., 2020), others experience the desertification of the Circum-Aral region that began in the 1960s (Saiko & Zonn, 2000), and yet other widespread land abandonment after the collapse of the Soviet Union in 1991 (de Beurs & Henebry, 2004; Kraemer et al., 2015; Lesiv et al., 2018; Prishchepov et al., 2013). Those changes have resulted in long-term changes in grassland vegetation cover and species composition, altered fire regimes (Dara et al., 2019; Dubinin et al., 2011; Freitag

et al., 2021) and shrub encroachment (Li et al., 2015). In Mongolia grasslands are threatened by intensified and often sedentary grazing replacing mobile pastoralism, which results in degradation and desertification (Meng et al., 2021; Sanzheev et al., 2020). Similarly, in Inner Mongolia of China, current grassland species composition and ecology reflect effects of the agricultural intensification that occurred between the early 1950s and late 1990s, followed by rewilding and afforestation initiated by the Great Green Wall and Grain for Green programs in late 1970s and 1999s, respectively (Chen et al., 2015; Song et al., 2014; Yin et al., 2018). Consequently, when analyzing changes in grassland cover in Eurasia it is necessary to recognize different ground cover trajectories of change to correctly attribute drivers, something that a change in "greenness" alone cannot capture.

Remote sensing data are well suited for grassland monitoring, including trend detection, due to their reliability and effectiveness for large-scale analysis, long-term image archives, and ability to capture even subtle changes (Ali et al., 2016; Dara et al., 2020; Reinermann et al., 2020). Vegetation indices derived based on active optical data are commonly used proxies for monitoring grassland vegetation cover, productivity and density (e.g., NDVI (Miao et al., 2021), LAI (Pasolli et al., 2015), or fPAR (Hobi et al., 2017)). Several analyses based on time series of remotely sensed data have identified increasing and decreasing trends in grassland vegetation productivity and green vegetation cover in Eurasia often referred to as "greening" and "browning," respectively (Cortés et al., 2021; de Beurs et al., 2015; de Jong et al., 2012). In Kazakhstan and the Russian part of the Caspian Lowlands, vegetation indices show "browning" trends in steppes according to long- (e.g., 1981–2006: de Jong et al. (2011); 1982–2008: de Jong et al. (2013); 1984–2017: Jiang et al. (2017)), medium- (e.g., 2000–2014: Zhang et al. (2021); and 2001–2013: de Beurs et al. (2015)), and short-term analyses (e.g., 2000–2008: de Beurs et al. (2009)). This "browning" has been attributed to climate variability (de Beurs et al., 2015; de Jong et al., 2013; Jiang et al., 2017) or the combination of climate and human activities (Zhang et al., 2021), though the effects of weather were not always statistically significant (de Beurs et al., 2009). Concurrently, grasslands in Mongolia and Eastern Mongolia are "greening," with the increase in productivity according to long- (e.g., 1982–2008: de Jong et al. (2012); 1985–2015: Miao et al. (2021)) and medium-term studies (e.g., 2000–2017: Chen et al. (2019); 2000–2016: Ding et al. (2020); and 2000–2014: Zhang et al. (2021)). The "greening" has also been attributed to climate (de Jong et al., 2013; Miao et al., 2021) and a combination of climate and anthropogenic activity (Zhang et al., 2021).



Unfortunately, the different trend analyses often show different change patterns and sometimes even contradicting trends for a given region (e.g., “browning” in central and northern Mongolia in Miao et al. (2021) based on a 1982–2015 time series, but not in Zhang et al. (2021) based on a 2000–2014 time series; or “browning” in NorthEastern Kazakhstan in de Beurs et al. (2015) based on a 2001–2013 time series, but not in Jiang et al. (2017) based on a 1984–2013 time series). The differences between identified trends may be due to differences in the timing and length of the observation records (Cortés et al., 2021) as well as due to different analytical approaches (Pan et al., 2018). Furthermore, although the long-term changes in grasslands in Eurasia have been extensively studied, most of the analyses are based on “one-dimensional” indices of photosynthetic activity (but see de Beurs et al., 2015; Hill & Guerschman, 2020), and do not account for temporal and spatial autocorrelation in the remotely sensed data. We sought to overcome both of these limitations here.

Spectral mixture analysis (SMA) quantifies all ground cover components of grassland cover (i.e., green vegetation, non-photosynthetic vegetation, soil, and shade), which characterize grassland conditions more comprehensively compared with vegetation indices (Masiliunas et al., 2021). Furthermore, spectral unmixing is advantageous in sparse vegetation conditions where soil reflectance affects vegetation indices (Elmore et al., 2000; Huete et al., 1985; Smith et al., 2019). Cumulative Endmember Fractions (CEFs), calculated as sums of endmember fractions over a period of 1 year, or a growing season (Lewińska et al., 2020, 2021), capture the full range of illumination conditions and phenology phases, and “normalize” those effects, which allows unbiased year-to-year comparisons. The “four-dimensional” information space of CEFs allows the identification of change trajectories (e.g., to separate a change from green vegetation to soil from a change from green vegetation to non-photosynthetic vegetation). To better capture trajectories, single fractions can be combined into ratios to illustrate transitions among fractions over time, which facilitates the mapping and understanding of change processes and their drivers.

Prior trend analyses of remotely sensed data have largely not accounted for temporal nor spatial autocorrelation leading to potentially incorrect conclusions (Ives et al., 2021). In per-pixel trend analyses, not accounting for temporal autocorrelation can lead to false positive identification of temporal trends (de Beurs & Henebry, 2004). Similarly, failing to account for spatial autocorrelation across the data (or a map), precludes recognition of true and statistically significant changes at the map scale (i.e., at the scale of the entire study area), which can result in both, false detection of clustered changes, and omission of subtle trends (Ives et al., 2021). Although the complications originating from autocorrelation in remotely sensed data are recognized (e.g., de Beurs et al., 2015; Tomaszewska et al., 2020; Zhou et al., 2001), few analyses have correctly accounted for it due to associated statistical and computational challenges (but see Bi et al., 2013; de Beurs et al., 2015; Xu et al., 2013). The Mann–Kendall test, despite frequent claim to the contrary, does not account at all for temporal

autocorrelation, and the seasonal Mann–Kendall test accounts only for temporal autocorrelation among seasons, but not among years (Hirsch & Slack, 1984).

Our goal was to investigate systematic trends in ground cover composition of grassland ecosystems in Eurasia while accounting for temporal and spatial autocorrelation in remotely sensed time series using the Partitioned Autoregressive Time Series (PARTS) approach (Ives et al., 2021). Specifically, our objectives were to: (i) calculate CEFs for all grassland-specific ground cover fractions (i.e., green vegetation, non-photosynthetic vegetation, soil, and shade) based on MODIS 2002–2020 time series; (ii) identify per-pixel systematic temporal trends in grassland ground cover depicting diverse trajectories of change and evaluate the range of spatial autocorrelation of these changes; and (iii) analyze the detected trends at map-scale, testing hypotheses about the effects of different independent environmental variables and their interactions (i.e., climate zone, country, elevation, land cover class, and SPEI3 (Standardized Precipitation–Evapotranspiration aggregated over 3 months)) on ground cover composition while accounting for spatial autocorrelation.

## 2 | MATERIALS AND METHODS

### 2.1 | Study area

The Eurasian grasslands (Figure 1) comprise 33 ecoregions from forest steppe to deserts (Olson et al., 2001) (Figure SA1), and represent 6 of 14 global biomes with a strong climate gradient from north to south (Figure SA2). In the northern part and in the mountain regions of the Pamir and the Tian Shan, climate is continental, but that changes toward the south into cold semiarid and cold desert. The mean annual temperature varies from  $-23^{\circ}\text{C}$  in the mountain regions to  $20^{\circ}\text{C}$  elsewhere. The maximum of the warmest month varies from  $10^{\circ}$  to  $40^{\circ}\text{C}$ , while the minimum of the coldest month varies from  $0^{\circ}$  to  $-35^{\circ}\text{C}$ . The annual precipitation ranges from 60 to 600 mm/year, with extreme values from almost 0 mm/year in the Taklamakan and Gobi Deserts to 1000 mm/year in the Pamir, the Tian Shan, and the Altai mountains (Beck et al., 2018; Karger et al., 2017).

The soils are mainly chernozems and dark kastanozems in the north, light-colored kastanozems in the center, and yermosols in the south (Figure SA3). Sandy soils, along with salty soils, are common in both the Aral and the Caspian depressions, and in the Kyzylkum, the Karakum, the Taklamakan, and the Gobi deserts. Lithosols are found in the mountains. The vegetation varies from forest steppe and meadow steppe (forbs) to shrubby deserts, depending on humidity, with some enclaves of boreal forests in the mountains.

In terms of land use, the west, northwest, and far northeast, where soil and weather conditions are the most favorable, are largely ploughed. Some enclaves of croplands are also located along larger rivers in the desert parts of the Eurasian grasslands (Hankerson et al., 2019; Sulla-Menashe et al., 2019). Abandoned fields are more common toward the south of the former Soviet republics

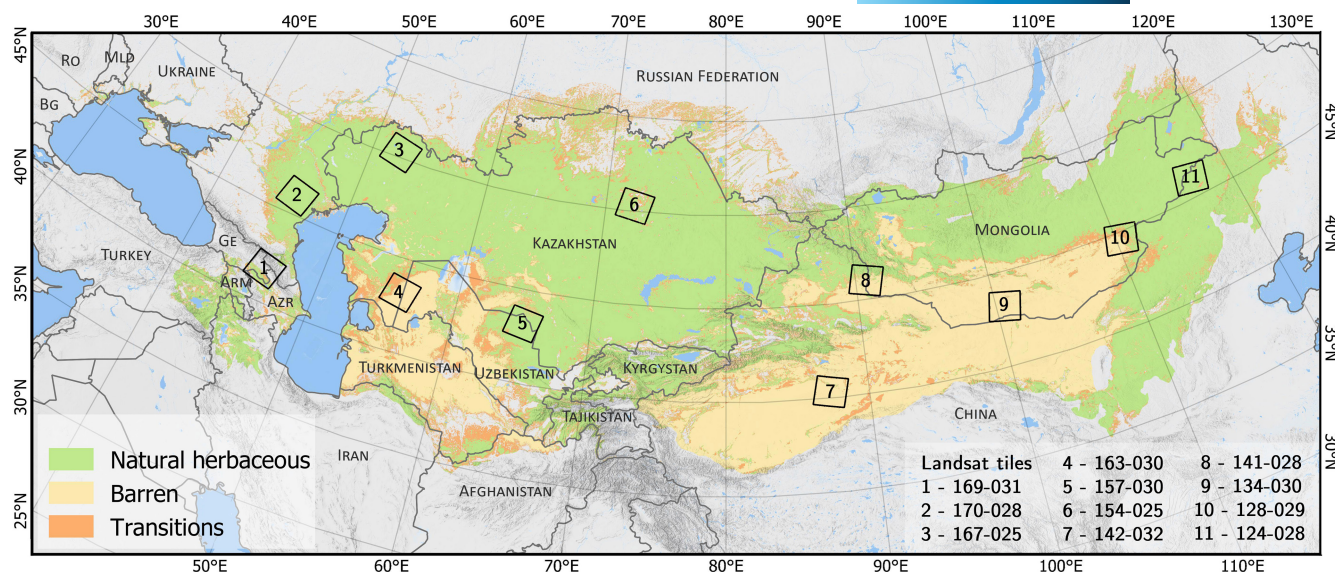


**FIGURE 1** Grasslands in Eurasia with respective land cover class based on the FAO LCCS 22001–2018 MCD12Q1 annual products. Note that map lines delineate study areas and do not necessarily depict accepted national boundaries. ARM, Armenia; AZR, Azerbaijan; BG, Bulgaria; GE, Georgia; MLD, Moldova; RO, Romania.

(Meyfroidt et al., 2016). Central Kazakhstan and most of Mongolia are covered by dry grasslands and used as pastures (Hankerson et al., 2019; Mongolian Statistics Office <http://www.en.nso.mn/>). The deserts or mountains of the South are also used as pastures or are depopulated.

## 2.2 | Earth observation data

We analyzed the 2002–2020 time series of the 8-day 500m MODIS surface spectral reflectance product (MOD09A1; Collection 6) available in Google Earth Engine (Gorelick et al., 2017; data accessed in March 2021) to calculate CEF (Lewńska et al., 2020, 2021). The data are atmospherically corrected (Vermote et al., 2002) and adjusted for sensor degradation (Lyapustin et al., 2014). We selected only high-quality pixels, and excluded clouds and snow (based on the “StateQA” band). We did not include data acquired prior to 2002 due to their lower quality.

To identify endmembers of ground cover fractions, which are essential to derive CEFs, we analyzed 55 Landsat scenes acquired between 2003 and 2019 in 11 footprints (Figure 1, Table SB1). When selecting footprints we prioritized those representing the predominantly arid climate of our study area, while ensuring representation of the main ecosystems, soil types, and country-specific conditions (Figures SA1–SA3). For each footprint, we selected cloud-free or nearly cloud-free scenes acquired during multi-year dry and wet spells (Figure SB1, Table SB1) as well as different phenological phases. This approach ensured a broad selection of vegetation and soil conditions, hence maximizing the diversity in our endmembers' pool. Suitable winter-time scenes were not available due to snow and cloud (Table SB1), but this did not hinder analyses due to the design of the CEF (Section 2.4). We downloaded all the Landsat data from the

U.S. Geological Survey (USGS) service (data accessed in November 2020) as collection 1 tier 1 surface reflectance products that were atmospherically corrected with LEDAPS (ETM+: Masek et al., 2006) or LaSRC (OLI: Vermote et al., 2016). We removed all pixels flagged as cloud, shadow, or snow according to the pixel quality assessment bands (Zhu & Woodcock, 2012). Finally, we adjusted the OLI scenes to ETM+ surface reflectance following Roy et al. (2016).

## 2.3 | Ancillary data

We adopted a broad definition of grasslands, that is, “grazing land” (FAO, 2005) and accordingly used the FAO LCC2 land cover classification available in the 2002–2019 MODIS MCD12Q1 product (Sulla-Menashe et al., 2019; Sulla-Menashe & Friedl, 2018) (data accessed in November 2020) to select which areas to focus on. Based on the land cover time series we identified pixels with stable “Natural Herbaceous” and “Barren” land cover, and assigned a “Transition” class when there was at least one change between these two classes between 2002 and 2019 (Figure 1). We included the barren class because it comprises areas up to 40% vegetation cover, many of which are used as pasture in Central Asia and Mongolia.

We used ancillary datasets to test hypotheses about the relations between environmental conditions and the observed trends in grassland ground cover composition in Eurasia. To characterize climate information we used the Köppen–Geiger climate classification (Kottek et al., 2006) (Figure SA2; 30 climate zones within our study area). We sourced elevation information from GTOPO30 dataset at 30 arc resolution (USGS, 1997) and incorporated administrative information at the country level as demarcated in FAO Global Administrative Unit Layers 2015 (FAO, 2015). We used monthly averaged precipitation and potential evapotranspiration from the

ERA5-Land ECMWF climate reanalysis data at 0.1 degree resolution (Muñoz Sabater, 2019) and calculated SPEI3 (Standardized Precipitation-Evapotranspiration Index calculated at the time scale of 3 months) (Vicente-Serrano et al., 2010, 2012) using the SPEI R library (<https://cran.r-project.org/web/packages/SPEI/>). We chose ERA5-Land due to its reliability in Central Asia (Zandler et al., 2020). All ancillary data were resampled to 500 m to match MODIS data using majority rule (for categorical data) and bilinear interpolation (for continuous data).

## 2.4 | Cumulative Endmember Fraction time series

For the SMA we identified four ground cover fractions characterizing grasslands, herein called endmembers: green vegetation, non-photosynthetic vegetation (i.e., dry leaves, shrub twigs), soil (or rock), and shade (i.e., vegetation micro-shadowing and topographic effect). Because 500-m resolution is too coarse to ensure spectrally pure pixels for endmember identification, we exploited in the similarity of spectral and orbital parameters of MODIS and Landsat (Gao et al., 2006; Hilker et al., 2009; Zhu et al., 2019). Following the methodology of Lewińska et al. (2020) we identified candidate “image endmembers” from Landsat images, making sure to cover a wide range of environmental and meteorological conditions across the study area (see Section 2.2, and Supplement B for details). By calculating the Minimum Noise Fraction and Pixel Purity Index for each selected Landsat scene, we identified and tested spectra of multiple soil types and green vegetation in different phenological stages (Table SB2). Additionally, we used the Ecological Spectral Information System (ECOSIS) Spectral Library (<https://ecosis.org>; accessed in May 2019) to add the non-photosynthetic vegetation endmember, which cannot be identified reliably from the Landsat images (Supplement B). We selected the set of final endmembers ensuring the lowest collinearity (Meer & Jia, 2012) and the lowest overall SMA RMSE, which quantifies how well endmembers explained the variance in the data (see Supplement B for details). Because our approach aims at quantifying the main ground cover characteristics of grasslands (i.e., green vegetation, non-photosynthetic vegetation, soil, and shade) and their change over time, rather than mapping the abundance of specific plant species, it allowed us to use more generically defined endmembers. The use of non-specie-specific endmembers definitions is common in SMA-based studies covering large grassland areas (Guerschman et al., 2015; Lewińska et al., 2020), and in other vegetation types (Bullock et al., 2018; Chen et al., 2021; Nill et al., 2022) because it allows to track changes in ground cover over time.

We applied the selected four endmembers in a constrained SMA model and ran it on each 8-day MODIS surface reflectance dataset available for 2002–2020 over Eurasia. Because MODIS band 5 has no equivalent in Landsat TM/ETM+, we excluded it from the SMA. We composited the resulting time series to monthly observations selecting from all corresponding 8-day datasets a set of

endmembers with the highest green vegetation fraction. Finally, we calculated pixel-based endmember-specific CEFs, that is, the sums of monthly fractions aggregated for the snow-free period of each year. We identified the pixel-specific snow-free period based on the 2002–2020 MODIS data taking the median of the first and last snow-free months to define the aggregation period (Figures SA4 and SA5, respectively). For each year we normalized the four CEFs on a per-pixel basis to conjointly sum up to 100%, allowing for straightforward comparison among years.

## 2.5 | Change trajectories in grassland ground cover composition

The design of the CEFs reflects a four-dimensional feature space with each of the ground cover types being represented by one axis used to describe the ground cover conditions. Because the sum of all ground cover fractions is constrained to be 100%, this feature space can be represented by a tetrahedron where at respective apexes each ground cover fraction reaches 100% coverage (Figure 2). Hence, by definition a change in one ground cover fraction results in a change in at least one other ground cover fraction. This principle applies to both a change in ground cover composition between two time-steps and long-term changes. It is possible to analyze changes in individual ground cover fractions, yet such an approach misses important aspects of the changes. Instead, it is advantageous to analyze the relationship between two or more fractions captured through ratios between fractions, which greatly facilitates interpretation of change trajectories. Because statistical distributions of ratios are often highly skewed, and were in our data too, we applied a logarithmic transformation to the response variables:

$$\text{ratio}_{ij_n} = \log \frac{e_{i_n} + c}{e_{j_n} + c}, \quad (1)$$

where  $e_i$  and  $e_j$  are CEFs for endmember  $i$  and  $j$ , respectively, in year  $n$ , and  $c$  is a small constant of 0.0001 (to prevent dividing by 0). Importantly, logarithmic transformation preserved the additive properties of our ratios allowing comparisons ( $\log \frac{x}{z} = \log \frac{x}{y} \times \frac{y}{z} = \log \frac{x}{y} + \log \frac{y}{z}$ ).

We first assessed overall long-term changes in vegetation cover, which we estimated as the trend in the sum of green and non-photosynthetic vegetation over soil CEFs ( $\frac{gv + npv}{soil}$ ). Subsequently, we analyzed positive trends in green vegetation (gv), non-photosynthetic vegetation (npv), and soil CEFs. Since positive and negative changes are interconnected among all fractions, we focus in our results on positive changes. Finally, we investigated trends in green vegetation in relation to non-photosynthetic vegetation ( $\frac{gv}{npv}$ ) and soil ( $\frac{gv}{soil}$ ), which allowed us to distinguish areas where the balance between green and dry vegetation fractions changed, irrespective of overall trends of either revegetation or desertification. Overall, the use of ratios allows for better understanding of the changes and their drivers (Table 1). Although some of the results were visually similar (e.g., gv and  $\frac{gv}{soil}$ ), the ratios

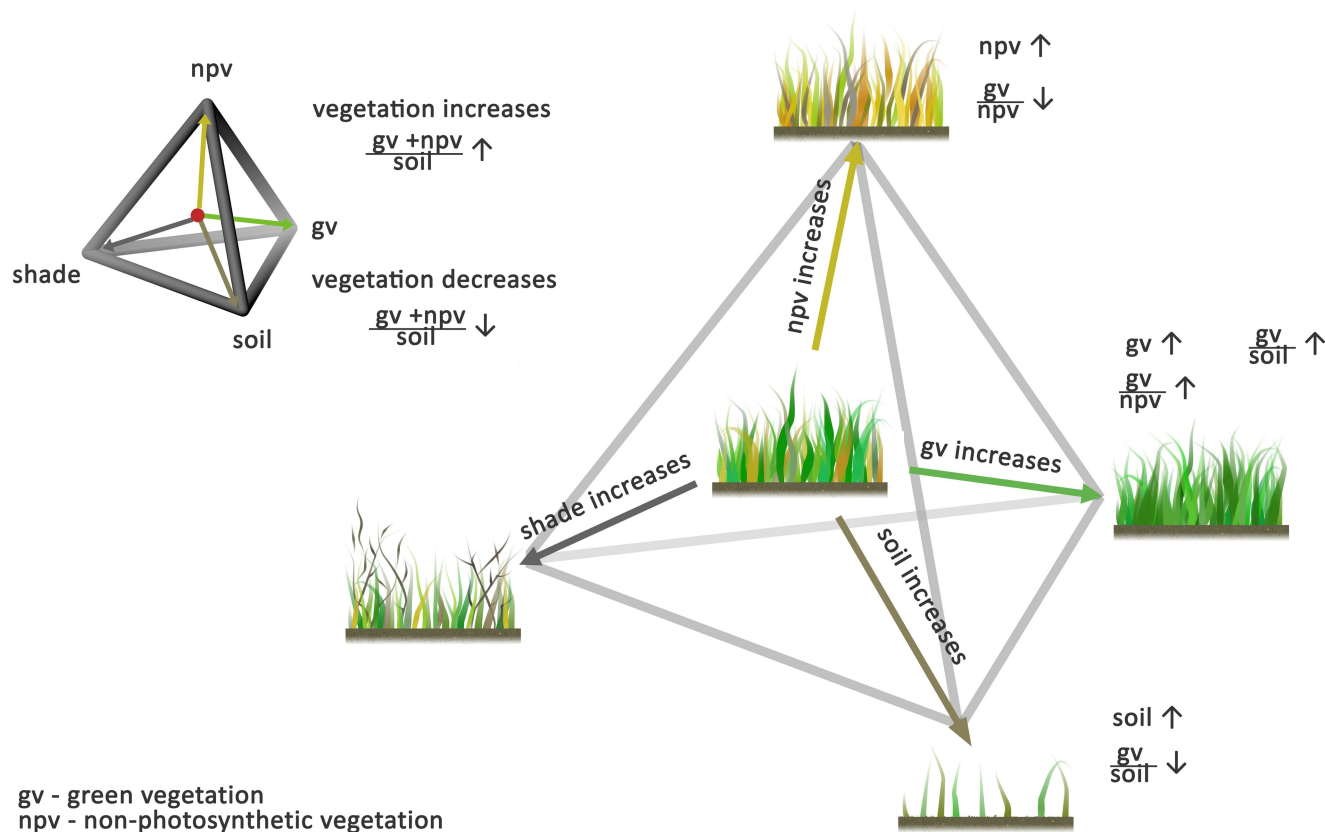


**FIGURE 2** Conceptual 4D feature space of the Cumulative Endmember Fractions in grasslands showing change trajectories in ground cover composition captured with single fractions and their ratios. For process-based meanings of the trajectories, see [Table 1](#).

**TABLE 1** Examples of process-based meanings of change trajectories in grassland ground cover composition.

Endmember	Increase	Decrease
gv	Increase in vegetation productivity or vegetation cover due to natural (e.g., revegetation) and anthropogenic factors (e.g., recultivation, cultivation practices) Change in species composition Longer vegetation season	Decrease in vegetation productivity or vegetation cover due to natural and anthropogenic factors (e.g., land abandonment, cultivation practices, grazing) Change in species composition Shorter vegetation season
npv	Desiccation due to natural (e.g., increasing aridity) and anthropogenic factors Overall increase in biomass leading to more dry matter in the senescence phase Change in species composition (e.g., shrub encroachment)	Desiccation due to natural (e.g., decreasing aridity) and anthropogenic factors Overall decrease in biomass leading to less dry matter in the senescence phase Change in species composition
soil	Increase in soil visibility due to natural (e.g., desertification) and anthropogenic factors (e.g., introduction or change in cultivation practices)	Decrease in soil visibility due to natural (e.g., revegetation) and anthropogenic factors (e.g., land abandonment, change in cultivation practices)
shade	Change in vegetation structure, for example, shrub encroachment Increase in soil crust	Change in vegetation structure, for example, reversing of shrub encroachment Decrease in soil crust

provide a quantitative assessment of specific change pathways (e.g., change in green vegetation in relation to soil) that single ground fractions do not capture, especially when testing map-scale statistical hypotheses as we intended (see [Section 2.6](#)). For clarity, we refer to the overall direction of changes in ground

cover composition using full names of fractions, that is, “green vegetation,” whereas when discussing a specific change trajectory we use the abbreviation, for example, gv. Finally, we present the shade ground cover fraction and all relevant results in the [Supplement A](#), section SA.1.



## 2.6 | PARTS: Accounting for temporal and spatial autocorrelation in trends

Developed by Ives et al. (2021, 2022) PARTS is a three-step statistical approach that allows for the analysis of trends in time series of raster data while accounting for temporal and spatial autocorrelation and in combination with additional covariates (e.g., meteorological data, or land cover information). First, by using an autoregressive model, PARTS derives temporally uncorrelated trends for each pixel in the time series. Second, using residuals from the autoregressive model PARTS estimates the spatial autocorrelation structure of the per-pixel trends. Third, PARTS conducts map-scale hypotheses about the relation between per-pixel trends and independent variables by performing a generalized least square (GLS) regression that takes into account the spatial autocorrelation structure of the per-pixel trends. This is a major advancement over prior methods because *p*-values of pixel-level trends give only a visual impression of the spatial patterns and cannot be used to evaluate overall significance of changes, due to spatial autocorrelation among pixels. Instead, the GLS step in PARTS includes per-pixel trends regardless of their individual *p*-values and derives statistically valid map-scale *p*-values for each tested hypothesis while accounting for spatial autocorrelation. Pixel-level trend maps can be useful to visualize the general spatial pattern of changes, but they are only an intermediate results. For a proper statistically meaningful interpretation pixel-level trends need to be analyzed with appropriate map-scale statistical tests that analyze all pixels simultaneously to obtain the greatest statistical power. PARTS is designed to do that.

### 2.6.1 | Temporal autocorrelation—Autoregressive trend analyses

To account for temporal autocorrelation in the time series, we followed PARTS of Ives et al. (2021), and estimated per-pixel time trends using autoregressive models implemented in the R package remotePARTS (<https://github.com/morrowcj/remotePARTS>). We separately analyzed trends in each single CEF and in the time series of the ratios. For each, we produced a pixel-based map depicting systematic trends and a map of the strength of temporal autocorrelation. For single CEFs we reported trends as percentage point change in abundance of a given fraction per year. For ratios, the trends represent qualitative and not quantitative information due to the logarithmic transformation of ratios. We used the autoregressive model implemented in remotePARTS to calculate per-pixel systematic trends in 2002–2020 SPEI3 time series aggregated to annual sums, which we used as an explanatory variable in the GLS regression analysis (Section 2.6.2).

### 2.6.2 | Spatial autocorrelation in time trends: Generalized least square regression

To investigate whether the spatial patterns of our trends could be explained by environmental variables, we tested map-scale

statistical hypotheses with GLS regressions that accounted for spatial autocorrelation. We defined the magnitude of the spatial correlation in each trend dataset as the unexplained variation in trends among pixels where the magnitude of autocorrelation depends on the distance between pixels (i.e., pixels located closer are more similar):

$$\text{cor}\{e_i, e_j\} = \text{nugget} + (1 - \text{nugget}) \exp\left(-\left(\frac{d_{ij}}{\text{range}}\right)^{\text{shape}}\right), \quad (2)$$

where  $\text{cor}\{e_i, e_j\}$  is the correlation between the random errors in pixels *i* and *j*,  $e_i$  and  $e_j$ ,  $d_{ij}$  is the distance between pixels, and nugget, range, and shape are parameters that determine the dependence of the correlation on distance. We calculated the range and shape of spatial correlation for each trend map, which give the distance beyond which two pixels are uncorrelated and the shape of the decay function, respectively (Ives et al., 2021, 2022).

We used this information in PARTS' GLS when we tested map-scale statistical hypotheses on the relation between the trends and the following explanatory variables: land cover (3 levels), climate zones (12 levels), countries (8 levels), elevation (continuous), and a temporally uncorrelated trend in SPEI3 (continuous). To examine changes in grasslands originating from regional land use legacies and policies, we further tested for statistical interactions between climate zone and country, land cover class and country, and SPEI3 trend and country factors. Due to the limited area of grasslands in some countries, we limited our country-specific analyses to China, Kazakhstan, Kyrgyzstan, Mongolia, Russia, Tajikistan, Turkmenistan, and Uzbekistan.

To overcome reduced statistical power arising from high correlation between adjacent pixels (Ives et al., 2021) we defined the magnitude and shape of spatial autocorrelation for each dataset and performed all subsequent GLS analyses using every third pixel in *x* and *y* direction of each map. Considering every third pixel aimed at preserving as much of the original data as possible, yet systematic sampling reduced data volume to about 11% of all pixels, which substantially accelerated the computations. Because remote PARTS divides the data points of the time trends in large remotely sensed data into random, non-overlapping partitions, then performs GLS regression on each partition and finally combines the statistical results from each partition (Ives et al., 2021, 2022), preserving as much as much of the original data as possible is critical for sufficient represent all factors' levels within each partition. Our tests showed that using a systematic subsample of a dataset has negligible impact on differences in the estimated range and shape of spatial autocorrelation (Table SA1).

Using PARTS' GLS allowed us to test for each trend map statistical hypotheses on the significance of the overall map-scale trend, and whether environmental variables explained spatial patterns of trends ( $H_0$ : there is no temporal trend in level *i*). For each model, we reported the trend within each level and checked for an overall effect of a given factor on the observed trends ( $H_0$ : factor *x* has no overall effect on trends). In all tests we used a significance threshold of  $p = .05$ .



### 3 | RESULTS

#### 3.1 | Cumulative Endmember Fractions

We successfully derived annual 2002–2020 CEFs for grasslands in Eurasia. The four endmembers that we selected for the SMA represented well the grassland ground cover fractions for the entire study area. The pixel-specific CEF aggregation period accounted for local phenological activity and excluded spurious values from the off-season. The per-pixel mean annual cumulative RMSE aggregated for the corresponding snow-free period rarely exceeded 1% reflectance, with the standard deviation not greater than 0.5% (Figure SA6), indicating how well our unmixing performed.

#### 3.2 | Trends in vegetation cover

Vegetation cover, estimated by relating the sum of green and non-photosynthetic vegetation to soil CEFs, was variable across Eurasia. At the pixel level, the  $\frac{gv + npv}{soil}$  ratio increased in Inner Mongolia and in the northern portion of our study area, especially in northern Kazakhstan (Figure 3). Decrease in vegetation cover occurred mainly in Central Asia, the Caspian Sea Depression, North of the Tian Shan Mountains, and the Taklamakan and Gobi Deserts. Notably, the range of spatial autocorrelation for this ratio was 136 km (Table 2), indicating that only pixels located further away are assumed statistically independent.

The overall changes in vegetation cover were insignificant at the map scale (Table 3), but changes in vegetation cover were positively related to changes in SPEI3 (Table 4). At the map scale, the increase in vegetation cover was significant in herbaceous grasslands (Table SA3), regions under diverse variants of cold climates (Table SA4), and in Kyrgyzstan and Russia (Table SA5). Moreover, we confirmed a significant increase in vegetation cover in cold climates

with dry winter and cold summers in China. We also found significant decreases in vegetation cover in cold climates without dry season in China, Kazakhstan, Kyrgyzstan and Russia, and in tundra areas in Kyrgyzstan and Russia (Table SA8). Individual factors had a significant overall effect on shaping trends in the  $\frac{gv + npv}{soil}$  ratio, but the effects of their interactions were insignificant.

#### 3.3 | Increase in green vegetation fraction

Positive trends in green vegetation fraction were widespread in Mongolia, China, northeastern Kazakhstan, and in the Tian Shan Mountains (Figures 4a and 5a,b). That pattern was apparent in  $gv$ , and in the  $\frac{gv}{soil}$  ratio time series. The pixel-level positive trends in the  $\frac{gv}{npv}$  ratio were the strongest in the Aral region (Figure 5a). The range of spatial autocorrelation in trends, which quantifies the maximum distance within which two observations are statistically dependent, was >110 km for  $gv$ , and around 50 and 33 km for  $\frac{gv}{soil}$  and  $\frac{gv}{npv}$ , respectively (Table 2).

The overall map-scale positive systematic trend in green vegetation fraction was significant only for the  $\frac{gv}{soil}$  ratio (Table 3). We found, however, a significant positive impact of elevation on  $gv$  trend (slope 0.096), and significant correlation between trends in  $gv$  and SPEI3 (0.089), and in the  $\frac{gv}{soil}$  ratio and SPEI3 (Table 4).

At the map scale, that is, across our entire study area, relations between environmental variables and spatial patterns in green vegetation trends were complex. Within the areas with herbaceous land cover we confirmed a significant increase in the  $\frac{gv}{soil}$  ratio, and so did we in the “Transition” class in the  $gv$  fraction (0.107; Table SA3). Concomitantly, increases in green vegetation fraction were significant in regions with cold and dry winters as indicated by positive changes in  $gv$  and  $\frac{gv}{soil}$ , as well as in cold climates without dry season according to the  $\frac{gv}{soil}$  ratio (Table SA4). When comparing the increase in green vegetation fraction among countries, we

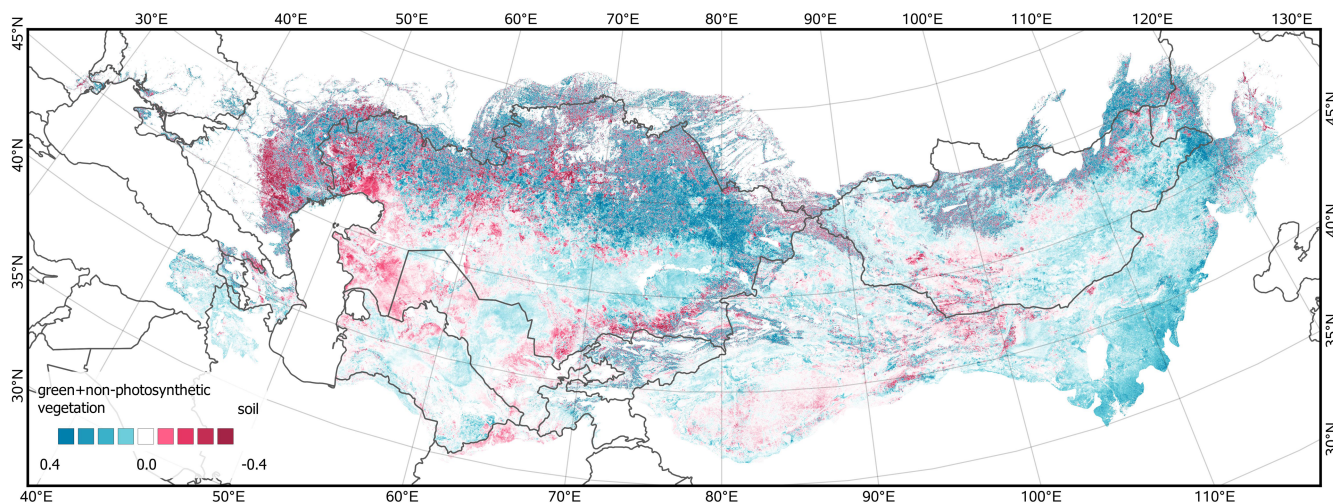


**FIGURE 3** Systematic trends in the ratio of the sum of green vegetation and non-photosynthetic vegetation over soil ( $\frac{gv + npv}{soil}$ ) Cumulative Endmember Fractions. Corresponding map with the strength of the temporal autocorrelation in Figure SA11, and map showing pixel-level trends with  $p < .05$  significance are presented in Figure SA7.

detected significant but small increasing trends in  $gv$  in China and Mongolia (0.091 and 0.093, respectively; Table SA5), and in  $\frac{gv}{soil}$  ratio in Kazakhstan, Kyrgyzstan, and in Russia. Importantly, increases in the  $\frac{gv}{soil}$  ratio were significantly related to an increase in SPEI3 in China, Kazakhstan, Mongolia, and Russia (Table SA6), whereas the increases in the  $\frac{gv}{npv}$  ratio were related to increase in SPEI3 in China and Mongolia. Although we found no significant increase in green vegetation fraction for the interactions of country and land cover (Table SA7), we did find significant increase in  $gv$  in cold and dry regions in China, Mongolia, and Tajikistan (Table SA8), and positive systematic changes in the  $\frac{gv}{npv}$  ratio in arid deserts and steppes in China, Kazakhstan, Kyrgyzstan, Turkmenistan, and Uzbekistan.

**TABLE 2** Range of spatial autocorrelation ( $r$ ) in trends in change trajectories in grassland ground cover composition.

Dataset	$r$ (km)
$gv$	110.41
$npv$	14.51
$soil$	11.53
$\frac{gv}{npv}$ ratio	33.50
$\frac{gv}{soil}$ ratio	49.86
$\frac{gv + npv}{soil}$ ratio	136.12

Abbreviations:  $gv$ , green vegetation;  $npv$ , non-photosynthetic vegetation.

**TABLE 3** Comparison of overall map-scale trends in change trajectories in grassland ground cover composition.

Dataset	Slope	Slope SE	t-val.	p-val.
$gv$	0.073	0.040	1.817	.069
$npv$	0.246	0.095	2.594	.009
$soil$	-0.218	0.100	-2.181	.029
$\frac{gv}{npv}$ ratio	-0.033	0.020	-1.630	.103
$\frac{gv}{soil}$ ratio	0.045	0.019	2.433	.015
$\frac{gv + npv}{soil}$ ratio	0.047	0.024	0.024	.052

Abbreviations:  $gv$ , green vegetation;  $npv$ , non-photosynthetic vegetation slope – slope of the trend; slope SE, slope standard error; t-val., t-test value; p-val., significance level of the slope.

**TABLE 4** Relationship between trends in change trajectories in grassland ground cover composition with elevation and SPEI3.

Dataset	Elevation				SPEI3			
	Slope	Slope SE	t-val.	p-val.	Slope	Slope SE	t-val.	p-val.
$gv$	0.096	0.040	2.384	.017	0.089	0.040	2.217	.027
$npv$	0.247	0.095	2.595	.009	0.248	0.096	2.595	.009
$soil$	-0.206	0.100	-2.054	.040	-0.276	0.101	-2.747	.006
$\frac{gv}{npv}$ ratio	-0.039	0.022	-1.750	.080	-0.031	0.021	-1.467	.142
$\frac{gv}{soil}$ ratio	0.031	0.020	1.572	.116	0.054	0.019	2.881	.004
$\frac{gv + npv}{soil}$ ratio	0.041	0.024	1.659	.097	0.060	0.024	2.491	.013

Note: Abbreviation as in Table 3.

Importantly, we confirmed a significant effect of our environmental variables and their interactions on changes in green vegetation fraction (Chi-square results in Tables SA3–SA8). The only exceptions were the  $\frac{gv}{soil}$  ratio for interactions between country and land cover, and the  $\frac{gv}{npv}$  for interaction between country and climate zone.

### 3.4 | Increase in non-photosynthetic vegetation fraction

Increasing trends in the non-photosynthetic vegetation fraction were abundant in Eurasia at the pixel level, and especially common in Central Asia and Inner Mongolia (Figure 4b), with the latter having the strongest  $npv$  trends. An increase in the amount of non-photosynthetic vegetation combined with decreases in photosynthetically active vegetation captured in the  $\frac{gv}{npv}$  ratio was widespread in Central Asia, the Gobi Desert, and in the mountains (Figure 5a). The range of spatial autocorrelation was of about 14 and 33 km for  $npv$  and  $\frac{gv}{npv}$  trends, respectively (Table 2).

Across Eurasia, we found a strong and significant overall map-scale increase in the  $npv$  fraction (Table 3; trend slope: 0.246). Moreover, both elevation and SPEI3 had positive relationships with changes in the  $npv$  fraction (Table 4; 0.247 and 0.248, respectively). The map-scale hypothesis testing confirmed the increase in non-photosynthetic fraction was significant across many factors' levels (Tables SA3–SA8). For example, the increase in  $npv$  was significant in the “transition” and herbaceous land cover, as was the decrease in the  $\frac{gv}{npv}$  ratio in barren and “transition” classes (Table SA3). Increasing trends in  $npv$  were significant and strong in arid deserts and steppe, in polar climates, and in areas with cold climate with no dry season, or dry summer (Table SA4). Conversely, decreasing trends in the  $\frac{gv}{npv}$  ratio were significant only in arid deserts (Table SA4). Our map-scale analyses confirmed significant positive trends in  $npv$  in all countries except Mongolia (Table SA5). Interestingly, in Russia the increase in  $npv$  was significantly related to negative changes in SPEI3, whereas in Uzbekistan increasing  $npv$  was associated with increasing SPEI3 (Table SA6). Negative trends in the  $\frac{gv}{npv}$  ratio were limited to China (Table SA5), where they were also significantly related with SPEI3 increases (Table SA6). We found significant increasing trends in  $npv$  for interactions between



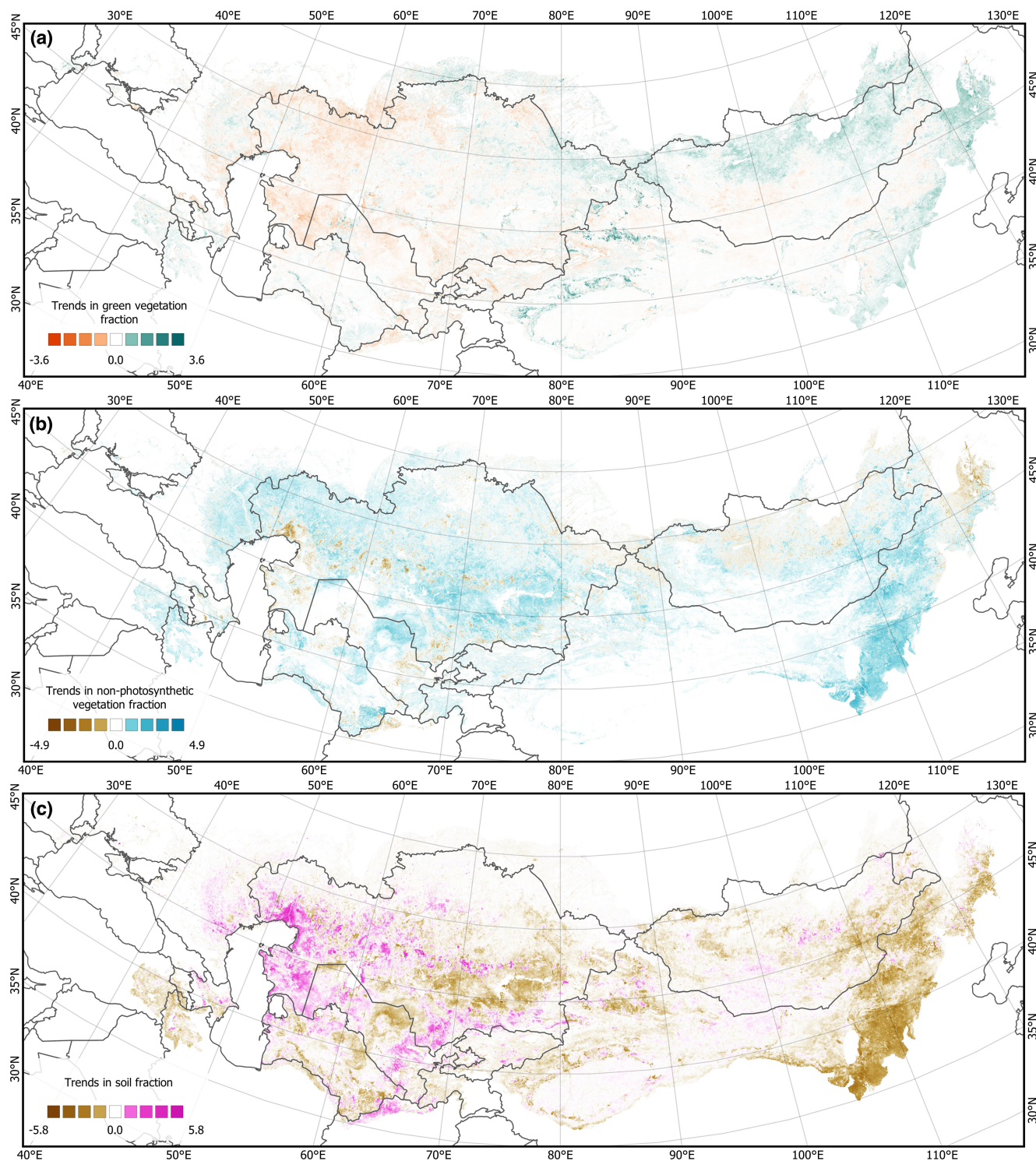


**FIGURE 4** Systematic trends in (a) green vegetation (gv), (b) non-photosynthetic vegetation (npv), and (c) soil (soil) Cumulative Endmember Fractions. The slope is reported in percentage points. Corresponding maps with the strength of temporal autocorrelation in [Figures SA11–SA13](#), respectively, and maps showing pixel-level trends with  $p < .05$  significance in [Figure SA7](#). Area statics for negative and positive trends are presented in [Table SA2](#).

country and land cover only in “transition” and herbaceous classes in Tajikistan and Turkmenistan ([Table SA7](#)). Map-scale npv trends for the interactions between country and climate were significant only in arid deserts in China, cold regions with dry and cold

summers in Kyrgyzstan, and in temperate climates with dry and hot summer in Turkmenistan ([Table SA8](#)). A Chi-square test confirmed insignificant differences between npv trends among countries, and the combination of country and climate (for npv and  $\frac{gv}{npv}$ ).



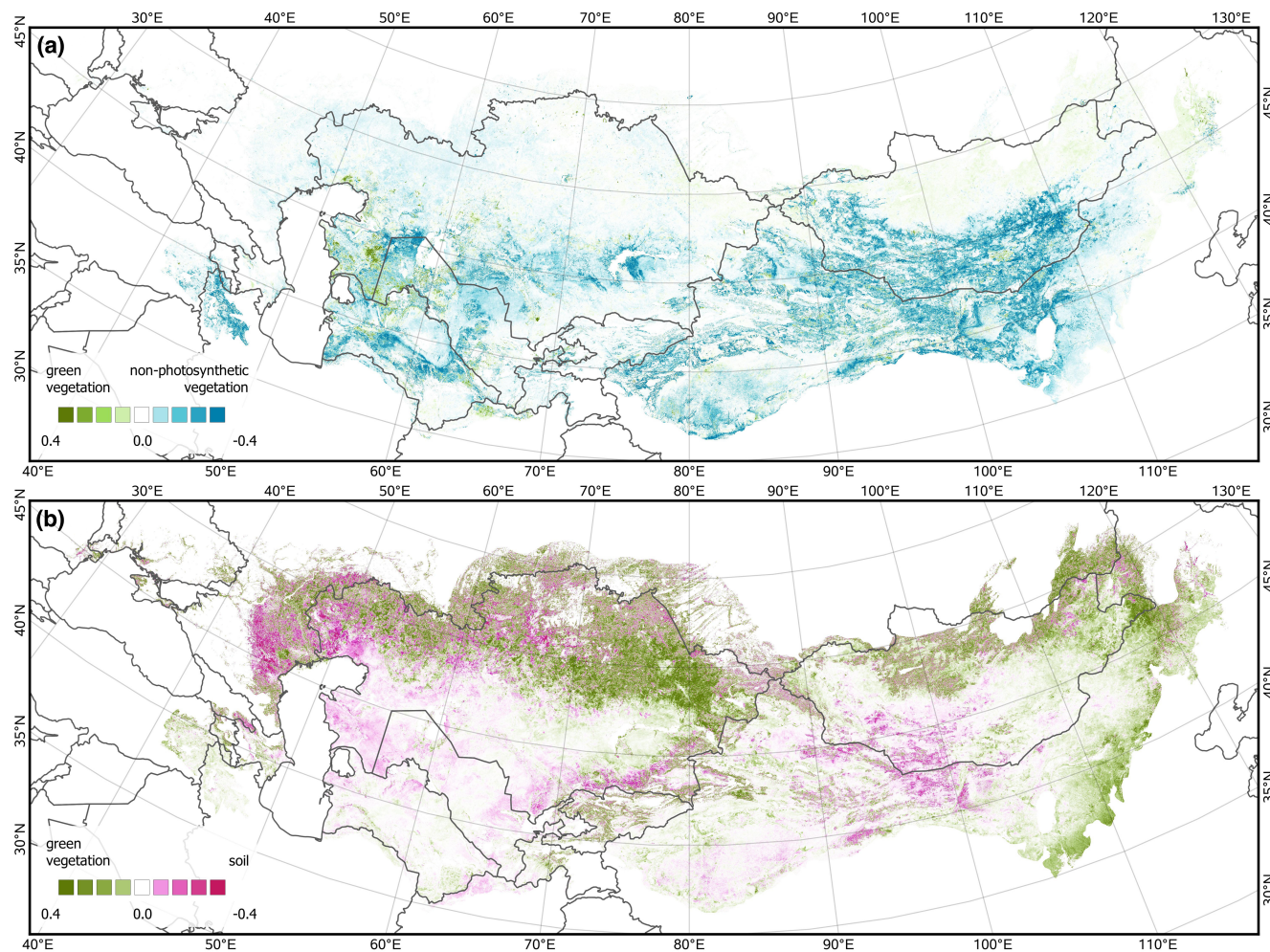


**FIGURE 5** Systematic trends in ratios of (a) green vegetation over non-photosynthetic vegetation ( $\frac{GV}{NPV}$ ) and (b) green vegetation over soil ( $\frac{GV}{S}$ ) Cumulative Endmember Fractions. Corresponding maps with the strength of temporal autocorrelation in [Figures SA14 and SA15](#), respectively, and maps showing pixel-level trends with  $p < .05$  significance in [Figure SA8](#).

### 3.5 | Decrease in vegetation cover

Increases in pixel-level abundance of soil fraction were most widespread in Central Asia, Caspian Sea Depression, and the Gobi Desert ([Figures 4c and 5b](#)). While positive trends in the soil fraction were often clustered, changes in the  $\frac{GV}{S}$  ratio were more dispersed, which was reflected in the range of spatial autocorrelation identified at around 12 and 50km, respectively ([Table 2](#)). We found no overall map-scale significant increase in the soil fraction abundance ([Table 3](#)), but higher elevation and SPEI3 were inversely related to the increase in soil fraction at the map scale ([Table 4](#); trend slope of  $-0.206$  and  $-0.276$ , respectively).

The increase in the soil fraction was insignificant at the map scale ([Tables SA3–SA8](#)). The only exception occurred in regions with a cold climate and dry and hot summers in Kazakhstan (for soil) and with a cold climate with no dry season and cold summer in Russia ( $\frac{GV}{S}$ , [Table SA8](#)). Notably, all environmental factors had a significant impact on trends in soil and  $\frac{GV}{S}$  when inspected separately. However, for factor's interaction, we found significant impacts only for

interactions between country and land cover for soil and between country and climate for  $\frac{GV}{S}$  ([Tables SA7 and SA8](#), respectively).

## 4 | DISCUSSION

We analyzed systematic trends in grasslands ground cover composition in Eurasia between 2002 and 2020 using ground cover fractions and statistical methods that directly account for temporal and spatial autocorrelation in the remotely sensed data. Across Eurasia, we found a statistically significant increase in non-photosynthetic vegetation, as well as localized increases in green vegetation. The wetter weather conditions after severe droughts in the late 1990s and early 2000s had significant effects on the overall increases in non-photosynthetic vegetation, increase in green vegetation combined with the decreases in the soil fraction in China, Kazakhstan, Mongolia, and Russia, and on the increases in green vegetation combined with the decrease in non-photosynthetic vegetation in Mongolia and China. We found

no statistical evidence for a map-level increase in the soil fraction across Eurasia. This shows that over the past 20 years there was an overall increase in vegetation cover in the grasslands of Eurasia, with grasslands now comprising greater non-photosynthetic fraction due to an overall increase in vegetation matter and potential shifts in vegetation type.

#### 4.1 | Increase in vegetation cover

Our results demonstrated interesting differences in the change pathways of vegetation cover when analyzed as green vegetation, non-photosynthetic vegetation, and the sum of both. Through hypothesis testing we rejected the hypothesis of an overall map-level increase in vegetation cover ( $\frac{gv + npv}{soil}$ ) and gv fraction, but confirmed significant increase in non-photosynthetic vegetation (npv) and increase in green vegetation paired with a decrease in soil ( $\frac{gv}{soil}$ ) (Table 3). This shows the importance of disentangling green and non-photosynthetic vegetation fractions and analyzing their specific change pathways separately. Although both fractions are closely related, and even though both together represent vegetation cover, the relation between gv and npv can alter due to successional changes in vegetation type or management practices (e.g., due to restoration programs like in China; Chen et al., 2015; Song et al., 2014; Yin et al., 2018). Consequently, we do not interpret the increase in non-photosynthetic vegetation, often detected as “browning,” as a clearly negative change, but rather as one of the change pathways in vegetative ground cover. The joint character of green and non-photosynthetic vegetation is further clarified by the positive map-scale effects of SPEI3 on the increases in green vegetation and non-photosynthetic vegetation, and their sum, but not on the  $\frac{gv}{npv}$  ratio (Table 4), which suggests that both fractions were similarly affected by meteorological conditions. The observed positive trends in vegetation-related fractions and their relation to SPEI3 may reflect a return to normal and wet weather conditions after the prolonged dry period in 1990s and 2000s (Guo et al., 2018; Sheffield et al., 2009).

Pixel-level increases in vegetation were common across Eurasia. Our trend maps showed strong  $\frac{gv + npv}{soil}$  increases in northern Kazakhstan, northern Mongolia, northeast China, and Inner Mongolia (Figure 3). When compared to other trend maps, the increase in vegetation was similar pixel-level positive trends in  $\frac{gv}{soil}$  and the increase in npv (Figures 4b and 5). Positive trends in gv, concentrated in the northern parts of our study area and in the mountains, also added to the overall pattern, though their contribution was less pronounced.

The overall footprint of our vegetation increase-related pathways corresponded well with the pixel-based “greening” patterns identified by de Jong et al. (2011, 2013), Jiang et al. (2017), Munier et al. (2018), Zhang et al. (2021), and Chen et al. (2019), but that greening was less pronounced in our maps. The difference is most likely due to our method accounting for temporal autocorrelations (Figures SA10, SA11, SA12, and SA15), but could also be due to

differences in metrics and study periods. Explicitly, the pixel-level increase in the  $\frac{gv}{soil}$  change trajectory in northeastern Kazakhstan corresponds with “greening” attributed to land abandonment (de Beurs & Henebry, 2004; Robinson, 2016), whereas “greening” in Mongolia, Inner Mongolia, and northeast China has been associated with beneficial combination of grazing and precipitation (Miao et al., 2021; Zhang et al., 2021) and land use changes arising from the Grain for Green reforms (Chen et al., 2015; Song et al., 2014; Yin et al., 2018). At the same time, the increase in the non-photosynthetic vegetation fraction, which was the most widespread change we detected at the pixel level (Figure 3), agreed with many areas previously identified as “browning” hotspots (de Beurs et al., 2009, 2015; de Jong et al., 2012, 2013; Ives et al., 2021; Jiang et al., 2017). Some differences among the patterns we attributed to a different “browning” definition, monitoring approach, length of the time series, and treatment of temporal autocorrelation (Figures SA12 and SA14).

However, not all of the pixel-level trends were significant at the map level. For example, the increase in  $\frac{gv + npv}{soil}$  ratio was significant only in Kyrgyzstan and Russia, gv was in China and Mongolia, whereas increasing trends in  $\frac{gv}{soil}$  were significant in Kazakhstan, Kyrgyzstan, and Russia (Table SA4). Concomitantly, the increase in npv was significant, strong, and uniform in all countries except Mongolia (Table SA5). Moreover, in China, Kazakhstan Mongolia, and Russia increasing trends in  $\frac{gv}{soil}$  matched positive changes in SPEI3 (Table SA6), which complements results from Jiang et al. (2017), Zhang et al. (2021) and Miao et al. (2021), and is likely due to vegetation recovery after severe droughts in late 1990s and early 2000s (Guo et al., 2018; Sheffield et al., 2009). Significant map-scale increases in photosynthetic activity in regions under cold climates align with easing of temperature-related vegetation growth limitations and a shift toward warmer and wetter conditions (Zhang et al., 2021) and with shorter snow seasons in the mountains (Tomaszewska & Henebry, 2018).

The distinction between the increase in green vegetation and non-photosynthetic vegetation was possible through the  $\frac{gv}{npv}$  ratio (Figure 5a). Although we found neither an overall map-level “greening” nor “browning” in Eurasia (Tables 3 and 4), map-level “browning” was statistically significant in barren areas, transitional grasslands (Table SA2), and arid cold deserts (Table SA4). Moreover, in China we found a surplus of non-photosynthetic vegetation over green vegetation (Table SA5), which was related to meteorological conditions (Table SA6), and may reflect a change in vegetation composition, such as shrub encroachment or afforestation, which have occurred in Central Asia, Northwest China (Li et al., 2015), the Tian Shan Mountains (Zhumanova et al., 2021), and Inner Mongolia (Bardgett et al., 2021; Hu & Nacun, 2018). At the pixel level, we found particularly good alignment of negative trends in the  $\frac{gv}{npv}$  ratio with “browning” detected during the last two decades, which could be due to suggested turning points in vegetation response from “greening” to “browning” (Horion et al., 2016; Li et al., 2015; Pan et al., 2018), or vegetation recovery after persistent dry spells in the late 1990s and early 2000s (Guo et al., 2018; Sheffield et al., 2009). Furthermore, our results are similar to the increase in non-photosynthetic



vegetation mapped by Hill and Guerschman (2020). Strong inter-annual autocorrelation in the  $\frac{gv}{npv}$  time series indicates a gradual process, typically associated with accumulation of dry vegetation matter and change in meteorological conditions.

## 4.2 | Decrease in vegetation cover

Prior studies suggested widespread grassland degradation and desertification in Eurasia (Cai et al., 2022; Hu et al., 2020; Zhang et al., 2018). However, our hypothesis tests found no significant map-scale decrease in vegetation combined with an increase in the soil fraction (Table 3) even though our trend maps showed pixel-level decrease in vegetation cover in favor of soil in Central Asia ( $\frac{gv + npv}{soil}$ , soil and  $\frac{gv}{soil}$ ), and the Gobi Desert ( $\frac{gv}{soil}$ ) (Figures 3, 4c, and 5b). Statistical tests showed that these trends were significant only in areas with cold climates in Kazakhstan, and in regions under cold climate with hot summers and without dry season in China, Russia, and Kyrgyzstan (Table SA8), which are typical for high mountains, such as the Altai Mountains and Caucasus.

Our pixel-level trend maps resembled to some extent the “browning” hotspots reported by Jiang et al. (2017), the decrease in vegetation indices and increase in Tasseled Cap brightness demonstrated by de Beurs et al. (2015), negative NDVI trends after 1998 observed by Li et al. (2015), and increases in bare soil mapped by Hill and Guerschman (2020). Overall, we expected to find only limited coincidence between our soil-specific results and generic “browning” maps, because most of the previous research considered “browning” as an overall decrease in vegetation indices, not an increase in soil presence, which is relatively sparse in Eurasia (Hu et al., 2020). As such, the detected pixel-based changes in soil,  $\frac{gv}{soil}$  and  $\frac{gv + npv}{soil}$  fractions corresponded best with desertification in Central Asia and Kazakhstan arising from agricultural exploitation and climate change (Cai et al., 2022; Hu et al., 2020), and salinization (Robinson, 2016; UNEP, 2011). The high inter-annual autocorrelation in the detected increase in soil fraction indicates the steadiness of desertification processes, presumably propelled by rising temperatures and aridity (Li et al., 2015). Furthermore, the small range of spatial autocorrelation and well-defined footprints of areas showing an increase in soil fraction may suggest land use drivers, such as localized overgrazing (Dara et al., 2020) and chemical degradation (Robinson, 2016). However, negative trends in the  $\frac{gv}{soil}$  and  $\frac{gv + npv}{soil}$  fractions may also indicate cropland expansion demonstrated by recultivation in northern Kazakhstan (Dara et al., 2018; Meyfroidt et al., 2016).

## 4.3 | Significance and limitations of the approach

We identified systematic changes in grasslands in Eurasia by applying a new and statistically rigorous approach. First, our approach is based on spectral unmixing, which provides physically based information on four grassland-specific ground cover fractions derived from multiple spectral bands. This is an advancement compared

with vegetation indices and allowed us to better analyze main characteristics of grassland ecosystems and their changes (Masiliunas et al., 2021). However, we acknowledge the potential limitations of SMA in separating soil and non-photosynthetic vegetation fractions (Kowalski et al., 2022) apparent in higher RMSE in regions with sparse vegetation cover (Figure SA6).

Second, by combining multiple ground cover fractions into ratios, we were able to identify distinct change trajectories better reflecting change processes. For example, ratio-based analyses permitted us to identify desertification-related changes constituting a decrease in vegetation accompanied by an increase in soil fraction. However, since various processes can result in the same change trajectory final process attribution still requires knowledge on local land use changes.

Third, by accounting for temporal autocorrelation at the pixel level our results give reliable pixel-based trends in ground cover fractions and their ratios. We found that temporal autocorrelation was very common in our time series (Figures SA10–SA15). When comparing the locations of autocorrelation hotspots in our data with the locations of long-term changes reported previously we noted a troublingly high degree of correspondence suggesting that some of the previously reported trends and hotspots may not be significant if they did not account for temporal autocorrelation.

Fourth, the range of spatial autocorrelation in the data varied between the datasets but was estimated consistently regardless of the spatial density of sample points (Table 2, Table SA1). This confirms the persistent character of spatial autocorrelation, the need to account for it, and highlights the spatial variability of different processes (e.g., wide-scale increase in  $gv$  vs. small-scale increase in soil fractions). Although the uniform range of spatial autocorrelation is a simplification, accounting for it in the PARTS' GLS regression allowed us to examine different map-scale statistical hypotheses. This is an important advancement because accounting for autocorrelation in the data both lends confidence to our results and demonstrates how the significance of the changes depends on the level of stratification and the hypothesis being tested (e.g., country vs. combination of country and climate zone).

Fifth, the PARTS method was designed specifically for regression-type analyses, identifying time trends in the response variable associated with explanatory variables. Therefore, PARTS makes it possible to predict changes in the response variable if there are changes in the future values of the environmental variables. PARTS, however, does not assess the unexplained variations in the data. Specifically, it does not assess whether areas of, for example, “browning” trends seen on a map will continue if they are not explained by environmental variables used in the regression analysis.

Finally, we focused in our presentation on the most commonly studied changes and change trajectories, and discussed only a subset of the results stemming from our analyses to maintain clarity of the manuscript. However, our approach provides opportunity to explore other change trajectories, such as changes in the shade fraction, which may indicate shrub encroachment and development of soil crust (Chen et al., 2005) (Supplement A).

## 5 | CONCLUSIONS

Our trend analyses showed that there was no significant decrease in vegetation cover in Eurasia over the past 20 years. On the contrary, the increase in non-photosynthetic vegetation fraction was by far the most widespread and statistically significant trend across Eurasia, and in all countries except Mongolia. Increases in green vegetation were more localized and moderate, but mostly significantly related to changes in meteorological conditions. Our results corroborate previous studies, especially those analyzing changes in Eurasian grasslands in the past two decades, but expand further upon the direction and character of changes, as well as the underlying process. Importantly, our state-of-the-art statistical approach accounting for temporal and spatial autocorrelation in the data ensures statistically robust assessment of the trends in the region. This is of great importance for understanding the changes and correct attribution of their drivers, especially considering recently arising ambiguity around trends analyses (Cortés et al., 2021; Ives et al., 2021). Furthermore, we tested a wide range of statistical hypotheses about the effect of different variables on changes in grasslands and found that all variables affected grasslands in Eurasia, but the map-scale significance of responses and relations varied greatly. This complexity highlights the wide range of change drivers and processes in grassland in Eurasia and thus the importance of an analysis design that allows for hypothesis testing. Lastly, our approach is scalable and transferable to other time series of satellite data and regions, and can be implemented in any computational environment, assuring accessibility and reproducibility.

## ACKNOWLEDGMENTS

We gratefully acknowledge support from the Advanced Information Systems Technology (AIST) program, grants NASAAIST-80NSSC20K0282, and the Land Cover and Land Use Change (LCLUC) Program of the National Aeronautic Space Administration (NASA), grants 80NSSC18K0316 and 80NSSC18K0343. We thank two anonymous reviewers for their constructive comments, which allowed us to greatly improve the manuscript.

## CONFLICT OF INTEREST STATEMENT

The authors declare that they have no known competing financial interests or personal relationships that could have influenced the work reported in this paper.

## DATA AVAILABILITY STATEMENT

The data that support the findings of this study are available in Dryads as <https://doi.org/10.5061/dryad.hmgqnk9nt> and at <https://silvis.forest.wisc.edu/data/eurasia-trends>. These data were derived from the MOD09A1 (Collection 6) data available in the public domain (<http://doi.org/10.5067/MODIS/MOD09A1.006>).

## ORCID

Katarzyna Ewa Lewińska  <https://orcid.org/0000-0001-6560-1235>

Anthony R. Ives  <https://orcid.org/0000-0001-9375-9523>  
 Clay J. Morrow  <https://orcid.org/0000-0002-3069-3296>  
 Natalia Rogova  <https://orcid.org/0000-0002-7779-6698>  
 He Yin  <https://orcid.org/0000-0002-2839-1723>  
 Paul R. Elsen  <https://orcid.org/0000-0002-9953-7961>  
 Kirsten de Beurs  <https://orcid.org/0000-0002-9244-3292>  
 Patrick Hostert  <https://orcid.org/0000-0002-5730-5484>  
 Volker C. Radeloff  <https://orcid.org/0000-0001-9004-221X>

## REFERENCES

- Ali, I., Cawkwell, F., Dwyer, E., Barrett, B., & Green, S. (2016). Satellite remote sensing of grasslands: From observation to management. *Journal of Plant Ecology*, 9(6), 649–671. <https://doi.org/10.1093/jpe/rtw005>
- Bardgett, R. D., Bullock, J. M., Lavorel, S., Manning, P., Ostle, N., Chomel, M., Durigan, G., Fry, E. L., Johnson, D., Lavelle, J. M., Le Provost, G., Luo, S., Png, K., Sankaran, M., Hou, X., Zhou, H., Ma, L., Ren, W., Li, X., ... Shi, H. (2021). Combatting global grassland degradation. *Nature Reviews Earth & Environment*, 2(10), 720–735. <https://doi.org/10.1038/s43017-021-00207-2>
- Baumann, M., Kamp, J., Pötzschner, F., Bleyhl, B., Dara, A., Hankerson, B., Prishchepov, A. V., Schierhorn, F., Müller, D., Hölzel, N., Krämer, R., Urazaliyev, R., & Kuemmerle, T. (2020). Declining human pressure and opportunities for rewilding in the steppes of Eurasia. *Diversity and Distributions*, 26, 1058–1070. <https://doi.org/10.1111/ddi.13110>
- Beck, H. E., Zimmermann, N. E., McVicar, T. R., Vergopolan, N., Berg, A., & Wood, E. F. (2018). Data Descriptor: Present and future Köppen-Geiger climate classification maps at 1-km resolution. *Nature Publishing Group*, 5, 1–12. <https://doi.org/10.1038/sdata.2018.214>
- Bengtsson, J., Bullock, J. M., Egoh, B., Everson, C., Everson, T., O'Connor, T., O'Farrell, P. J., Smith, H. G., & Lindborg, R. (2019). Grasslands—More important for ecosystem services than you might think. *Ecosphere*, 10(2). <https://doi.org/10.1002/ecs2.2582>
- Bi, J., Xu, L., Samanta, A., Zhu, Z., & Myneni, R. (2013). Divergent arctic-boreal vegetation changes between North America and Eurasia over the past 30 years. *Remote Sensing*, 5, 2093–2112. <https://doi.org/10.3390/rs5052093>
- Bullock, E. L., Woodcock, C. E., & Olofsson, P. (2018). Monitoring tropical forest degradation using spectral unmixing and Landsat time series analysis. *Remote Sensing of Environment*, 238(April), 110968. <https://doi.org/10.1016/j.rse.2018.11.011>
- Cai, D., Wang, X., Jiao, L., & Geng, X. (2022). Baseline and status of desertification in Central Asia. *Land Degradation & Development*, 33(November 2021), 771–784. <https://doi.org/10.1002/ldr.4214>
- Chen, C., Park, T., Wang, X., Piao, S., Xu, B., Chaturvedi, R. K., Fuchs, R., Brovkin, V., Ciais, P., Fensholt, R., Tømmervik, H., Bala, G., Zhu, Z., Nemani, R. R., & Myneni, R. B. (2019). China and India lead in greening of the world through land-use management. *Nature Sustainability*, 2(February), 122–129. <https://doi.org/10.1038/s41893-019-0220-7>
- Chen, H., Marter-kenny, J., López-carr, D., & Liang, X. (2015). Land cover and landscape changes in Shaanxi Province during China's Grain for Green Program (2000–2010). *Environmental Monitoring and Assessment*, 187, 1–14. <https://doi.org/10.1007/s10661-015-4881-z>
- Chen, J., Yuan, M., Wang, L., Shimazaki, H., & Tamura, M. (2005). A new index for mapping lichen-dominated biological soil crusts in desert areas. *Remote Sensing of Environment*, 96, 165–175. <https://doi.org/10.1016/j.rse.2005.02.011>
- Chen, S., Woodcock, C. E., Bullock, E. L., Ar, P., Service, U. S. F., & Mountain, R. (2021). Monitoring temperate forest degradation on Google Earth Engine using Landsat time series analysis. *Remote Sensing of Environment*, 265, 112648. <https://doi.org/10.1016/j.rse.2021.112648>

- Cherlet, M., Hutchinson, C., Reynolds, J., Hill, J., Sommer, S., & von Maltitz, G. (Eds.). (2018). *World atlas of desertification*. Publication Office of the European Union. <https://doi.org/10.2760/9205>
- Cortés, J., Mahecha, M. D., & Reichstein, M. (2021). Where are global vegetation greening and browning trends significant? *Geophysical Research Letters*, 48, e2020GL091496. <https://doi.org/10.1029/2020GL091496>
- Cowie, A. L., Orr, B. J., Castillo Sanchez, V. M., Chasek, P., Crossman, N. D., Erlewein, A., Louwagie, G., Maron, M., Metternicht, G. I., Minelli, S., Tengberg, A. E., & Welton, S. (2018). Land in balance: The scientific conceptual framework for Land Degradation Neutrality. *Environmental Science and Policy*, 79(November 2017), 25–35. <https://doi.org/10.1016/j.envsci.2017.10.011>
- Dara, A., Baumann, M., Freitag, M., Hölzel, N., Hostert, P., Kamp, J., Müller, D., Prishchepov, A. V., & Kuemmerle, T. (2020). Annual Landsat time series reveal post-Soviet changes in grazing pressure. *Remote Sensing of Environment*, 239(April 2019), 111667. <https://doi.org/10.1016/j.rse.2020.111667>
- Dara, A., Baumann, M., Hölzel, N., Hostert, P., Kamp, J., Müller, D., Ullrich, B., & Kuemmerle, T. (2019). Post-Soviet land-use change affected fire regimes on the Eurasian Steppes. *Ecosystems*, 23, 943–956. <https://doi.org/10.1007/s10021-019-00447-w>
- Dara, A., Baumann, M., Kuemmerle, T., Pflugmacher, D., Rabe, A., Griffiths, P., Hölzel, N., Kamp, J., Freitag, M., & Hostert, P. (2018). Mapping the timing of cropland abandonment and recultivation in northern Kazakhstan using annual Landsat time series. *Remote Sensing of Environment*, 213(September 2017), 49–60. <https://doi.org/10.1016/j.rse.2018.05.005>
- de Beurs, K. M., Wright, C. K., & Henebry, G. M. (2009). Dual scale trend analysis for evaluating climatic and anthropogenic effects on the vegetated land surface in Russia and Kazakhstan. *Environmental Research Letters*, 4(4). <https://doi.org/10.1088/1748-9326/4/4/045012>
- de Beurs, K. M., & Henebry, G. M. (2004). Land surface phenology, climatic variation, and institutional change: Analyzing agricultural land cover change in Kazakhstan. *Remote Sensing of Environment*, 89(4), 497–509. <https://doi.org/10.1016/j.rse.2003.11.006>
- de Beurs, K. M., Henebry, G. M., Owsley, B. C., & Sokolik, I. (2015). Using multiple remote sensing perspectives to identify and attribute land surface dynamics in Central Asia 2001–2013. *Remote Sensing of Environment*, 170, 48–61. <https://doi.org/10.1016/j.rse.2015.08.018>
- de Jong, R., De Bruin, S., De Wit, A., Schaepman, M. E., & Dent, D. L. (2011). Analysis of monotonic greening and browning trends from global NDVI time-series. *Remote Sensing of Environment*, 115(2), 692–702. <https://doi.org/10.1016/j.rse.2010.10.011>
- de Jong, R., Schaepman, M. E., Furrer, R., de Bruin, S., & Verbarg, P. H. (2013). Spatial relationship between climatologies and changes in global vegetation activity. *Global Change Biology*, 19(6), 1953–1964. <https://doi.org/10.1111/gcb.12193>
- de Jong, R., Verbesselt, J., Schaepman, M. E., & de Bruin, S. (2012). Trend changes in global greening and browning: Contribution of short-term trends to longer-term change. *Global Change Biology*, 18(2), 642–655. <https://doi.org/10.1111/j.1365-2486.2011.02578.x>
- De Keersmaecker, W., Lhermitte, S., Tits, L., & Honnay, O. (2015). A model quantifying global vegetation resistance and resilience to short-term climate anomalies and their relationship with vegetation cover. *Global Change Biology*, 20, 2149–2161. <https://doi.org/10.1111/gcb.12279>
- Ding, C., Huang, W., Li, Y., Zhao, S., & Huang, F. (2020). Nonlinear changes in dryland vegetation greenness over East Inner Mongolia, China, in recent years. *Sensors*, 20(3839), 1–14.
- Dubinin, M., Luschekina, A., & Radeloff, V. C. (2011). Climate, livestock, and vegetation: What drives fire increase in the arid ecosystems of southern Russia? *Ecosystems*, 14(4), 547–562. <https://doi.org/10.1007/s10021-011-9427-9>
- Elmore, A. J., Mustard, J. F., Manning, S. J., & Lobell, D. B. (2000). Quantifying vegetation change in semiarid environments: Precision and accuracy of spectral mixture analysis and the normalized difference vegetation index. *Remote Sensing of Environment*, 102(March 1999), 87–102. [https://doi.org/10.1016/S0034-4257\(00\)00100-0](https://doi.org/10.1016/S0034-4257(00)00100-0)
- FAO. (2005). *Grasslands of the world* (J. M. Suttie, S. G. Reynolds, & C. Batello, Eds.) (Vol. 2005). Food and Agricultural Organization of the United Nations. <https://search.library.wisc.edu/catalog/9910012077802121>
- FAO. (2015). *Global Administrative Unit Layers (GAUL)*. Food and Agriculture Organization of the United Nations (FAO). <http://www.fao.org/geonetwork>
- Freitag, M., Kamp, J., Dara, A., Kuemmerle, T., Sidorova, T. V., Stirnemann, I. A., Velbert, F., & Hölzel, N. (2021). Post-Soviet shifts in grazing and fire regimes changed the functional plant community composition on the Eurasian steppe. *Global Change Biology*, 27(July 2020), 388–401. <https://doi.org/10.1111/gcb.15411>
- Gao, F., Masek, J., Schwaller, M., & Hall, F. (2006). On the blending of the MODIS and Landsat ETM + surface reflectance: Predicting daily Landsat surface reflectance. *IEEE Transactions on Geoscience and Remote Sensing*, 44(8), 2207–2218. <https://doi.org/10.1109/TGRS.2006.872081>
- Gorelick, N., Hancher, M., Dixon, M., Ilyushchenko, S., Thau, D., & Moore, R. (2017). Google Earth engine: Planetary-scale geospatial analysis for everyone. *Remote Sensing of Environment*, 202, 18–27. <https://doi.org/10.1016/j.rse.2017.06.031>
- Guerschman, J. P., Scarth, P. F., McVicar, T. R., Renzullo, L. J., Malthus, T. J., Stewart, J. B., Rickards, J. E., & Trevithick, R. (2015). Assessing the effects of site heterogeneity and soil properties when unmixing photosynthetic vegetation, non-photosynthetic vegetation and bare soil fractions from Landsat and MODIS data. *Remote Sensing of Environment*, 161, 12–26. <https://doi.org/10.1016/j.rse.2015.01.021>
- Guo, H., Bao, A., Liu, T., Jiapaer, G., Ndayisaba, F., & Jiang, L. (2018). Spatial and temporal characteristics of droughts in Central Asia 1966–2015. *Science of the Total Environment*, 624, 1523–1538. <https://doi.org/10.1016/j.scitotenv.2017.12.120>
- Hankerson, B. R., Schierhorn, F., Prishchepov, A. V., Dong, C., Eisfelder, C., & Mu, D. (2019). Modeling the spatial distribution of grazing intensity in Kazakhstan. *PLoS ONE*, 2050, 1–27.
- Hilker, T., Wulder, M. A., Coops, N. C., Linke, J., McDermid, G., Masek, J. G., Gao, F., & White, J. C. (2009). A new data fusion model for high spatial- and temporal-resolution mapping of forest disturbance based on Landsat and MODIS. *Remote Sensing of Environment*, 113(8), 1613–1627. <https://doi.org/10.1016/j.rse.2009.03.007>
- Hill, M. J., & Guerschman, J. P. (2020). The MODIS global vegetation fractional cover product 2001–2018: Characteristics of vegetation fractional cover in grasslands and savanna woodlands. *Remote Sensing*, 12(3). <https://doi.org/10.3390/rs12030406>
- Hirsch, R. M., & Slack, J. R. (1984). A nonparametric trend test for seasonal data with serial dependence. *Water Resources Research*, 20(6), 727–732.
- Hobi, M. L., Dubinin, M., Graham, C. H., Coops, N. C., Clayton, M. K., Pidgeon, A. M., & Radeloff, V. C. (2017). A comparison of Dynamic Habitat Indices derived from different MODIS products as predictors of avian species richness. *Remote Sensing of Environment*, 195, 142–152. <https://doi.org/10.1016/j.rse.2017.04.018>
- Horion, S., Prishchepov, A. V., Verbesselt, J., de Beurs, K., Tagesson, T., & Fensholt, R. (2016). Revealing turning points in ecosystem functioning over the Northern Eurasian agricultural frontier. *Global Change Biology*, 22(8), 2801–2817. <https://doi.org/10.1111/gcb.13267>
- Hu, Y., Han, Y., & Zhang, Y. (2020). Land desertification and its influencing factors in Kazakhstan. *Journal of Arid Environments*, 180(April), 104203. <https://doi.org/10.1016/j.jaridenv.2020.104203>
- Hu, Y., & Nacun, B. (2018). An analysis of land-use change and grassland degradation from a policy perspective in Inner Mongolia, China,

- 1990–2015. *Sustainability*, 10. <https://doi.org/10.3390/su10114048>
- Huete, A. R., Jackson, R. D., & Post, D. F. (1985). Spectral response of a plant canopy with different soil backgrounds. *Remote Sensing of Environment*, 17(1), 37–53. [https://doi.org/10.1016/0034-4257\(85\)90111-7](https://doi.org/10.1016/0034-4257(85)90111-7)
- IPBES. (2018). *The IPBES assessment report on land degradation and restoration*. Companion to Environmental Studies. <https://doi.org/10.4324/9781315640051-105>
- IPCC. (2019). *Special report on climate change and land*. IPCC. <https://www.ipcc.ch/report/srcccl/>
- Ives, A. R., Zhu, L., Wang, F., Zhu, J., Morrow, C. J., & Radeloff, C. (2021). Statistical inference for trends in spatiotemporal data. *Remote Sensing of Environment*, 266(September), 112678. <https://doi.org/10.1016/j.rse.2021.112678>
- Ives, A. R., Zhu, L., Wang, F., Zhu, J., Morrow, C. J., & Radeloff, V. C. (2022). Statistical tests for non-independent partitions of large autocorrelated datasets. *MethodsX*, 9, 101660. <https://doi.org/10.1016/j.mex.2022.101660>
- Jiang, L., Jiapaer, G., Bao, A., Guo, H., & Ndayisaba, F. (2017). Vegetation dynamics and responses to climate change and human activities in Central Asia. *Science of the Total Environment*, 599–600, 967–980. <https://doi.org/10.1016/j.scitotenv.2017.05.012>
- Karch, F., Jerzy, F., & Timoshenko, V. P. (1964). *Soviet Agricultural Policy, 1953–1962*. Food Research Institute Studies.
- Karger, D. N., Conrad, O., Böhner, J., Kawohl, T., Kreft, H., Soria-Auza, R. W., Zimmermann, N. E., Linder, P., & Kessler, M. (2017). Data Descriptor: Climatologies at high resolution for the earth's land surface areas. *Nature Publishing Group*, 4, 1–20. <https://doi.org/10.1038/sdata.2017.122>
- Kerven, C., Robinson, S., & Behnke, R. (2021). Pastoralism at scale on the Kazakh rangelands: From clans to workers to ranchers. *Frontiers in Sustainable Food Systems*, 4(January), 1–21. <https://doi.org/10.3389/fsufs.2020.590401>
- Kottek, M., Grieser, J., Beck, C., Rudolf, B., & Rubel, F. (2006). World Map of the Köppen-Geiger climate classification updated. *Meteorologische Zeitschrift*, 15(3), 259–263. <https://doi.org/10.1127/0941-2948/2006/0130>
- Kowalski, K., Okujeni, A., Brell, M., & Hostert, P. (2022). Quantifying drought effects in Central European grasslands through regression-based unmixing of intra-annual Sentinel-2 time series. *Remote Sensing of Environment*, 268(November 2021), 112781. <https://doi.org/10.1016/j.rse.2021.112781>
- Kraemer, R., Prishchepov, A. V., Müller, D., Kuemmerle, T., Radeloff, V. C., Dara, A., Terekhov, A., & Frühauf, M. (2015). Long-term agricultural land-cover change and potential for cropland expansion in the former Virgin Lands area of Kazakhstan. *Environmental Research Letters*, 10. <https://doi.org/10.1088/1748-9326/10/5/054012>
- Lesiv, M., Schepaschenko, D., Moltchanova, E., Bun, R., Dürauer, M., Prishchepov, A. V., Schierhorn, F., Estel, S., Kuemmerle, T., Alcántara, C., Kussul, N., Shchepashchenko, M., Kutovaya, O., Martynenko, O., Karminov, V., Shvidenko, A., Havlik, P., Kraxner, F., See, L., & Fritz, S. (2018). Data descriptor: Spatial distribution of arable and abandoned land across former Soviet Union countries. *Scientific Data*, 5, 1–12. <https://doi.org/10.1038/sdata.2018.56>
- Lewińska, K. E., Buchner, J., Bleyhl, B., & Hostert, P. (2021). Changes in the grasslands of the Caucasus based on Cumulative Endmember Fractions from the full 1987–2019 Landsat record. *Science of Remote Sensing*, 4. <https://doi.org/10.1016/j.srs.2021.100035>
- Lewińska, K. E., Hostert, P., Buchner, J., Bleyhl, B., & Radeloff, V. C. (2020). Short-term vegetation loss versus decadal degradation of grasslands in the Caucasus based on Cumulative Endmember Fractions. *Remote Sensing of Environment*, 248(June), 111969. <https://doi.org/10.1016/j.rse.2020.111969>
- Li, Z., Chen, Y., Li, W., Deng, H., & Fang, G. (2015). Potential impacts of climate change on vegetation dynamics in Central Asia. *Journal of Geophysical Research: Atmospheres*, 120, 12345–12356. <https://doi.org/10.1002/2015JD023618>
- Lioubimtseva, E., & Henebry, G. M. (2009). Climate and environmental change in arid Central Asia: Impacts, vulnerability, and adaptations. *Journal of Arid Environments*, 73(11), 963–977. <https://doi.org/10.1016/j.jaridenv.2009.04.022>
- Lorenz, K., & Lal, R. (2018). Carbon sequestration in grassland soils. In *Carbon sequestration in agricultural ecosystems* (pp. 175–209). Springer International Publishing. [https://doi.org/10.1007/978-3-319-92318-5\\_4](https://doi.org/10.1007/978-3-319-92318-5_4)
- Lyapustin, A., Wang, Y., Xiong, X., Meister, G., Platnick, S., Levy, R., Franz, B., Korkin, S., Hilker, T., Tucker, J., Hall, F., Sellers, P., Wu, A., & Angal, A. (2014). Scientific impact of MODIS C5 calibration degradation and C6+ improvements. *Atmospheric Measurement Techniques*, 7, 4353–4365. <https://doi.org/10.5194/amt-7-4353-2014>
- Masek, J. G., Vermote, E. F., Saleous, N. E., Wolfe, R., Hall, F. G., Huemmrich, K. F., Gao, F., Kutler, J., & Lim, T. K. (2006). A landsat surface reflectance dataset for North America, 1990–2000. *IEEE Geoscience and Remote Sensing Letters*, 3(1), 68–72. <https://doi.org/10.1109/LGRS.2005.857030>
- Masilunas, D., Tsendbazar, N., Herold, M., Lesiv, M., Buchhorn, M., & Verbesselt, J. (2021). Global land characterisation using land cover fractions at 100 m resolution. *Remote Sensing of Environment*, 259(March), 112409. <https://doi.org/10.1016/j.rse.2021.112409>
- Meer, F. D. V. D., & Jia, X. (2012). Collinearity and orthogonality of endmembers in linear spectral unmixing. *International Journal of Applied Earth Observation and Geoinformation*, 18, 491–503. <https://doi.org/10.1016/j.jag.2011.10.004>
- Meng, X., Gao, X., Li, S., Li, S., & Lei, J. (2021). Monitoring desertification in Mongolia based on Landsat images and Google Earth Engine from 1990 to 2020. *Ecological Indicators*, 129, 107908. <https://doi.org/10.1016/j.ecolind.2021.107908>
- Meyfroidt, P., Schierhorn, F., Prishchepov, A. V., Müller, D., & Kuemmerle, T. (2016). Drivers, constraints and trade-offs associated with recultivating abandoned cropland in Russia, Ukraine and Kazakhstan. *Global Environmental Change*, 37, 1–15. <https://doi.org/10.1016/j.gloenvcha.2016.01.003>
- Miao, L., Sun, Z., Müller, D., Ren, Y., & Schierhorn, F. (2021). Grassland greening on the Mongolian Plateau despite higher grazing intensity. *Land Degradation & Development*, 32(September 2020), 792–802. <https://doi.org/10.1002/ldr.3767>
- Munier, S., Carrer, D., Planque, C., & Camacho, F. (2018). Satellite leaf area index: Global scale analysis of the tendencies per vegetation type over the last 17 years. *Remote Sensing*, 10(424), 1–25. <https://doi.org/10.3390/rs10030424>
- Muñoz Sabater, J. (2019). ERA5-Land monthly averaged data from 1981 to present. Copernicus Climate Change Service (C3S) Climate Data Store (CDS). <https://doi.org/10.24381/cds.68d2bb3>
- Ni, J. (2002). Carbon storage in grasslands of China. *Journal of Arid Environments*, 50, 205–218. <https://doi.org/10.1006/jare.2001.0902>
- Nill, L., Grünberg, I., Ullmann, T., Gessner, M., Boike, J., & Hostert, P. (2022). Arctic shrub expansion revealed by Landsat-derived multitemporal vegetation cover fractions in the Western Canadian Arctic. *Remote Sensing of Environment*, 281(September), 113228. <https://doi.org/10.1016/j.rse.2022.113228>
- Olson, A., David, M., Eric, D., Neil, D., & George, V. N. (2001). Terrestrial ecoregions of the world: A new map of life on earth. *BioScience*, 51(11), 933–938.
- O'Mara, F. P. (2012). The role of grasslands in food security and climate change. *Annals of Botany*, 110(6), 1263–1270. <https://doi.org/10.1093/aob/mcs209>
- Pan, N., Feng, X., Fu, B., Wang, S., Ji, F., & Pan, S. (2018). Increasing global vegetation browning hidden in overall vegetation greening: Insights from time-varying trends. *Remote Sensing of Environment*, 214(May), 59–72. <https://doi.org/10.1016/j.rse.2018.05.018>



- Panunzi, E. (2008). *Are grasslands under threat?* FAO. [www.fao.org/uploads/media/grass\\_stats\\_1.pdf](http://www.fao.org/uploads/media/grass_stats_1.pdf)
- Passolli, L., Asam, S., Castelli, M., Bruzzone, L., Wohlfahrt, G., Zebisch, M., & Notarnicola, C. (2015). Retrieval of Leaf Area Index in mountain grasslands in the Alps from MODIS satellite imagery. *Remote Sensing of Environment*, 165, 159–174. <https://doi.org/10.1016/j.rse.2015.04.027>
- Prishchepov, A. V., Schierhorn, F., Dronin, N., Ponkina, E. V., & Müller, D. (2020). 800 years of agricultural land-use change in Asian (Eastern) Russia. In M. Frühauf, G. Guggenberger, T. Meinel, I. Theesfeld, & S. Lentz (Eds.), *KULUNDA: Climate smart agriculture: South Siberian agro-steppe as pioneering region for sustainable land use* (pp. 67–87). Springer International Publishing. [https://doi.org/10.1007/978-3-030-15927-6\\_6](https://doi.org/10.1007/978-3-030-15927-6_6)
- Prishchepov, A. V., Müller, D., Dubinin, M., Baumann, M., & Radeloff, V. C. (2013). Determinants of agricultural land abandonment in post-Soviet European Russia. *Land Use Policy*, 30(1), 873–884. <https://doi.org/10.1016/j.landusepol.2012.06.011>
- Reinermann, S., Asam, S., & Kuenzer, C. (2020). Remote sensing of grassland production and management—A review. *Remote Sensing*, 12(12). <https://doi.org/10.3390/rs12121949>
- Robinson, S. (2016). Land degradation in Central Asia: Evidence, perception and policy. In R. Behnke & M. Mortimore (Eds.), *The end of desertification?: Disputing environmental change in the drylands* (pp. 451–490). Springer Berlin Heidelberg. [https://doi.org/10.1007/978-3-642-16014-1\\_17](https://doi.org/10.1007/978-3-642-16014-1_17)
- Rolinski, S., Prishchepov, A. V., Guggenberger, G., Bischoff, N., Kurganova, I., Schierhorn, F., Müller, D., & Müller, C. (2021). Dynamics of soil organic carbon in the steppes of Russia and Kazakhstan under past and future climate and land use. *Regional Environmental Change*, 21, 73. <https://doi.org/10.1007/s10113-021-01799-7>
- Roy, D. P., Kovalsky, V., Zhang, H. K., Vermote, E. F., Yan, L., Kumar, S. S., & Egorov, A. (2016). Characterization of Landsat-7 to Landsat-8 reflective wavelength and normalized difference vegetation index continuity. *Remote Sensing of Environment*, 185, 57–70. <https://doi.org/10.1016/j.rse.2015.12.024>
- Saiko, T. A., & Zonn, I. S. (2000). Irrigation expansion and dynamics of desertification in the Circum-Aral region of Central Asia. *Applied Geography*, 20, 349–367.
- Sanzheev, E. D., Mikheeva, A. S., Osodoev, P. V., Batomunkuev, V. S., & Tulokhonov, A. K. (2020). Theoretical approaches and practical assessment of socio-economic effects of desertification in Mongolia. *International Journal of Environmental Research and Public Health*, 17, 4068. <https://doi.org/10.3390/ijerph17114068>
- Sheffield, J., Andreadis, K. M., Wood, E. F., & Lettenmaier, D. P. (2009). Global and continental drought in the second half of the twentieth century: Severity—Area—Duration analysis and temporal variability of large-scale events. *Journal of Climate*, 22, 1962–1981. <https://doi.org/10.1175/2008JCLI2722.1>
- Smelansky, I. E., & Tishkov, A. A. (2012). The Steppe biome in Russia: Ecosystem services, conservation status, and actual challenges. In *Eurasian Steppes. Ecological problems and livelihoods in a changing world* (pp. 45–101). <https://doi.org/10.1007/978-94-007-3886-7>
- Smith, W. K., Dannenberg, M. P., Yan, D., Herrmann, S., Barnes, M. L., Barron-Gafford, G. A., Biederman, J. A., Ferrenberg, S., Fox, A. M., Hudson, A., Knowles, J. F., MacBean, N., Moore, D. J. P., Nagler, P. L., Reed, S. C., Rutherford, W. A., Scott, R. L., Wang, X., & Yang, J. (2019). Remote sensing of dryland ecosystem structure and function: Progress, challenges, and opportunities. *Remote Sensing of Environment*, 233(August), 111401. <https://doi.org/10.1016/j.rse.2019.111401>
- Song, X., Peng, C., Zhou, G., Jiang, H., & Wang, W. (2014). Chinese Grain for Green Program led to highly increased soil organic carbon. *Scientific Reports*, 4, 1–7. <https://doi.org/10.1038/srep04460>
- Sulla-Menashe, D., & Friedl, M. A. (2018). User guide to collection 6 MODIS land cover (MCD12Q1 and MCD12C1) product. USGS, 1–18. <https://doi.org/10.5067/MODIS/MCD12Q1>
- Sulla-Menashe, D., Gray, J. M., Abercrombie, S. P., & Friedl, M. A. (2019). Hierarchical mapping of annual global land cover 2001 to present: The MODIS Collection 6 Land Cover product. *Remote Sensing of Environment*, 222(April 2018), 183–194. <https://doi.org/10.1016/j.rse.2018.12.013>
- Tomaszewska, M., & Henebry, G. (2018). Changing snow seasonality in the highlands of Kyrgyzstan. *Environmental Research Letters*, 13, 065006. <https://doi.org/10.1088/1748-9326/aabd6f>
- Tomaszewska, M. A., Nguyen, L. H., & Henebry, G. M. (2020). Land surface phenology in the highland pastures of montane Central Asia: Interactions with snow cover seasonality and terrain characteristics. *Remote Sensing of Environment*, 240(December 2019), 111675. <https://doi.org/10.1016/j.rse.2020.111675>
- UN General Assembly. (2021). *Resolution adopted by the General Assembly on 1 March 2019 [A/73/L.76 and A/73/L.76/Add.1 United Nations Decade on Ecosystem Restoration (2021–2030)]* (Vol. 03519).
- UNEP. (2011). *Caspian Sea State of the Environment*. Encyclopedia of Environment and Society. <http://hdl.handle.net/20.500.11822/9712>
- USGS. (1997). *USGS 30 ARC-second Global Elevation Data, GTOPO30*. Research Data Archive at the National Center for Atmospheric Research, Computational and Information Systems Laboratory. <https://doi.org/10.5065/A1Z4-EE71>
- Vermote, E., Justice, C., Claverie, M., & Franch, B. (2016). Preliminary analysis of the performance of the Landsat 8/OLI land surface reflectance product. *Remote Sensing of Environment*, 185, 46–56. <https://doi.org/10.1016/j.rse.2016.04.008>
- Vermote, E. F., El Saleous, N. Z., & Justice, C. O. (2002). Atmospheric correction of MODIS data in the visible to middleinfrared: First results. *Remote Sensing of Environment*, 83, 97–111. [https://doi.org/10.1016/S0034-4257\(02\)00089-5](https://doi.org/10.1016/S0034-4257(02)00089-5)
- Vicente-Serrano, S. M., Beguería, S., & López-Moreno, J. I. (2010). A multiscalar drought index sensitive to global warming: The standardized precipitation evapotranspiration index. *Journal of Climate*, 23(7), 1696–1718. <https://doi.org/10.1175/2009JCLI2909.1>
- Vicente-Serrano, S. M., Beguería, S., Lorenzo-Lacruz, J., Camarero, J. J., López-Moreno, J. I., Azorin-Molina, C., Revuelto, J., Morán-Tejeda, E., & Sanchez-Lorenzo, A. (2012). Performance of drought indices for ecological, agricultural, and hydrological applications. *Earth Interactions*, 16(10), 1–27. <https://doi.org/10.1175/2012EI000434.1>
- Winkler, K., Fuchs, R., Rounsevell, M., & Herold, M. (2021). Global land use changes are four times greater than previously estimated. *Nature Communications*, 12, 2501. <https://doi.org/10.1038/s41467-021-22702-2>
- Xu, L., Myneni, R. B., Iii, F. S. C., Callaghan, T. V., Pinzon, J. E., Tucker, C. J., Zhu, Z., Bi, J., Ciais, P., Tømmervik, H., Euskirchen, E. S., Forbes, B. C., Piao, S. L., Anderson, B. T., Ganguly, S., Nemani, R. R., Goetz, S. J., Beck, P. S. A., Bunn, A. G., ... Stroeve, J. C. (2013). Temperature and vegetation seasonality diminishment over northern lands. *Nature Climate Change*, 3(March), 581–586. <https://doi.org/10.1038/nclimate1836>
- Yin, H., Pflugmachera, D., Li, A., Li, Z., & Hostert, P. (2018). Land use and land cover change in Inner Mongolia—Understanding the effects of China's re-vegetation programs. *Remote Sensing of Environment*, 204(October 2017), 918–930. <https://doi.org/10.1016/j.rse.2017.08.030>
- Zandler, H., Senftl, T., & Vanselow, K. A. (2020). Reanalysis datasets outperform other gridded climate products in vegetation change analysis in peripheral conservation areas of Central Asia. *Scientific Reports*, 10, 22446. <https://doi.org/10.1038/s41598-020-79480-y>
- Zhang, G., Biradar, C. M., Xiao, X., Dong, J., Zhou, Y., Qin, Y., Zhang, Y., Liu, F., Ding, M., & Thomas, R. J. (2018). Exacerbated grassland degradation and desertification in Central Asia during 2000–2014. *Ecological Applications*, 28(2), 442–456. <https://doi.org/10.1002/eap.1660>
- Zhang, Y., Wang, Q., Wang, Z., Li, J., & Xu, Z. (2021). Dynamics and drivers of grasslands in the Eurasian Steppe during 2000–2014. *Sustainability*, 13. <https://doi.org/10.3390/su13115887>



- Zhou, L., Tucker, C. J., Kaufmann, R. K., Slayback, D., Shabanov, N. V., & Myneni, R. B. (2001). Variations in northern vegetation activity inferred from satellite data of vegetation index during 1981 to 1999. *Journal of Geographical Research*, 106, 20069–20083.
- Zhu, L., Ives, A. R., Zhang, C., Guo, Y., & Radeloff, V. C. (2019). Climate change causes functionally colder winters for snow cover-dependent organisms. *Nature Climate Change*, 9, 886–893. <https://doi.org/10.1038/s41558-019-0588-4>
- Zhu, Z., & Woodcock, C. E. (2012). Object-based cloud and cloud shadow detection in Landsat imagery. *Remote Sensing of Environment*, 118, 83–94. <https://doi.org/10.1016/j.rse.2011.10.028>
- Zhumanova, M., Wrage-mönnig, N., & Jurasinski, G. (2021). Science of the Total Environment Long-term vegetation change in the Western Tien-Shan Mountain pastures, Central Asia, driven by a combination of changing precipitation patterns and grazing pressure. *Science of the Total Environment*, 781, 146720. <https://doi.org/10.1016/j.scitotenv.2021.146720>

## SUPPORTING INFORMATION

Additional supporting information can be found online in the Supporting Information section at the end of this article.

**How to cite this article:** Lewińska, K. E., Ives, A. R., Morrow, C. J., Rogova, N., Yin, H., Elsen, P. R., de Beurs, K., Hostert, P., & Radeloff, V. C. (2023). Beyond “greening” and “browning”: Trends in grassland ground cover fractions across Eurasia that account for spatial and temporal autocorrelation. *Global Change Biology*, 29, 4620–4637. <https://doi.org/10.1111/gcb.16800>